Check for updates

Paleoceanography and Paleoclimatology

RESEARCH ARTICLE
10.1029/2025PA005364

A Tropically Hot Late Jurassic North American Sundance Sea: Evidence for the Oxfordian Warm Interval

R. W. Reynolds[1], R. Jerrett[2], A. Marca[3], M. Davies[1], S. M. Bernasconi[4], R. B. Paxton[3], G. Nowell[5], P. Dennis[3], U. Balthasar[1], and G. D. Price[1]

[1]School of Geography, Earth and Environmental Sciences, University of Plymouth, Plymouth, UK, [2]School of Earth and Environmental Sciences, University of St. Andrews, St. Andrews, UK, [3]School of Environmental Sciences, University of East Anglia, Norwich, UK, [4]Department of Earth and Planetary Sciences, ETH Zürich, Zurich, Switzerland, [5]Department of Earth Sciences, University of Durham, Durham, UK

Key Points:

- Unusually high mid-latitude sea-surface temperatures during the Oxfordian, with a mean of 30.6°C
- For the southern Sundance Sea, $\delta^{18}O$ seawater values ranged from −2.3‰ to −0.1‰ with a basin average of −1.3‰
- Radiogenic enrichment of $^{87}Sr/^{86}Sr$ of ~2.5×10^{-5} in the Sundance Sea relative to the Oxfordian open-ocean

Supporting Information:

Supporting Information may be found in the online version of this article.

Correspondence to:

R. W. Reynolds,
rhicert.reynolds@plymouth.ac.uk

Citation:

Reynolds, R. W., Jerrett, R., Marca, A., Davies, M., Bernasconi, S. M., Paxton, R. B., et al. (2026). A tropically hot Late Jurassic North American Sundance Sea: Evidence for the Oxfordian warm interval. *Paleoceanography and Paleoclimatology*, *41*, e2025PA005364. https://doi.org/10.1029/2025PA005364

Received 31 OCT 2025
Accepted 20 JUL 2026

Author Contributions:

Conceptualization: R. W. Reynolds, G. D. Price
Data curation: R. W. Reynolds
Formal analysis: R. W. Reynolds, A. Marca, M. Davies, S. M. Bernasconi, R. B. Paxton, G. Nowell, P. Dennis, G. D. Price
Funding acquisition: G. D. Price
Investigation: R. W. Reynolds, R. Jerrett, G. D. Price
Methodology: R. W. Reynolds, A. Marca, M. Davies, S. M. Bernasconi, P. Dennis
Project administration: G. D. Price
Resources: R. W. Reynolds, G. D. Price
Supervision: R. Jerrett, A. Marca, P. Dennis, U. Balthasar, G. D. Price

© 2026 The Author(s). Paleoceanography and Paleoclimatology published by Wiley Periodicals LLC on behalf of American Geophysical Union.
This is an open access article under the terms of the Creative Commons Attribution License, which permits use, distribution and reproduction in any medium, provided the original work is properly cited.

Abstract The Late Jurassic greenhouse climate was characterized by elevated atmospheric CO_2 (pCO_2) at 600–1,000 ppm and sea-surface temperatures substantially warmer than today. These conditions peaked during the Oxfordian, when extensive epicontinental seaways, including the North American Sundance Sea, dominated mid-latitude paleoceanography. We present clumped isotope (Δ_{47}) and $^{87}Sr/^{86}Sr$ analyses of Oxfordian belemnite and *Gryphaea* fossils from the Sundance Sea to reconstruct paleotemperatures ($t\Delta_{47}$) and assess the balance between open ocean and terrestrial inputs. The data reveal (a) a mean $t\Delta_{47}$ of 30.6°C (±1.6 1SE), or 27.6°C (±1.6 1SE) if subjected to maximum bond reordering, reflecting unusually high mid-latitude sea-surface temperatures; (b) $\delta^{18}O$ seawater values ranging from −2.3‰ (±1.5 1SE) to −0.1‰ (±0.7 1SE) within the Sundance Sea; and, (c) evidence of a slight radiogenic enrichment in $^{87}Sr/^{86}Sr$ (0.706850, offset by 2.0×10^{-5} to 3.0×10^{-5}) relative to the reconstructed global seawater curve for the early-mid Oxfordian, indicating a limited connectivity between the Sundance Sea and Panthalassic Ocean. When integrated with existing Jurassic Δ_{47} records, these findings provide evidence for an Oxfordian Warm Interval and locally elevated sea-surface temperatures in the Sundance Sea relative to the coeval open ocean, owing to its marginal or semi-enclosed hydrography. This furthermore demonstrates the capacity of the Δ_{47} proxy to resolve the upper thermal bounds of Jurassic greenhouse climates.

Plain Language Summary During the Late Jurassic period, Earth's climate was much warmer than it is today, with higher atmospheric CO_2 and hotter sea surface temperatures. During this period, large shallow seas, like the Sundance Sea in North America, covered parts of many continents. Fossils from the Sundance Sea are used to reconstruct ancient temperatures and understand the seaway's water chemistry. The results show that the average sea surface temperature was about 30.6°C, much warmer than today's mid-latitudes. Seawater composition indicates variable local conditions, although the semi-enclosed Sundance Sea's connectivity with the open ocean enabled marine conditions to persist. These findings confirm the Oxfordian as a particularly warm interval and highlight how fossil evidence helps us understand extreme climate conditions during the Jurassic.

1. Introduction

1.1. Environmental Context

The Late Jurassic represents a warm period with high pCO_2 at c. 600–1,000 ppm (Foster et al., 2017), and elevated global oceanic temperatures between c. 21°–30°C (Jenkyns et al., 2012; Wang et al., 2025) lasting around 12 million years. A feature of this warmer world was the presence of large epicontinental seaways, such as the Mid to Late Jurassic (Bathonian to Oxfordian, c. 168.2–154.8 Ma; International Commission on Stratigraphy, 2024) Sundance Sea in North America, which was located at mid-latitudes between c. 35°–60°N (Paleolatitude, 2025). At its greatest extent, it stretched from modern-day Utah to the Arctic Ocean (Danise et al., 2020; Schueth et al., 2025; Zuchuat et al., 2022) (Figure 1). As much of the Jurassic oceanic crust has since been subducted (Seton et al., 2012; Stampfli & Borel, 2002), these epicontinental seaways are the dominant source for much of our information about ancient marine climates and biodiversity throughout the Jurassic (Massare et al., 2013; Parcell & Williams, 2005; Schwarz et al., 2022; Sellwood & Jenkyns, 1975) and have the potential to inform the limits of extreme climates in the geological record.

Validation: R. W. Reynolds, S. M. Bernasconi
Visualization: R. W. Reynolds
Writing – original draft: R. W. Reynolds
Writing – review & editing: R. Jerrett, A. Marca, M. Davies, S. M. Bernasconi, P. Dennis, U. Balthasar, G. D. Price

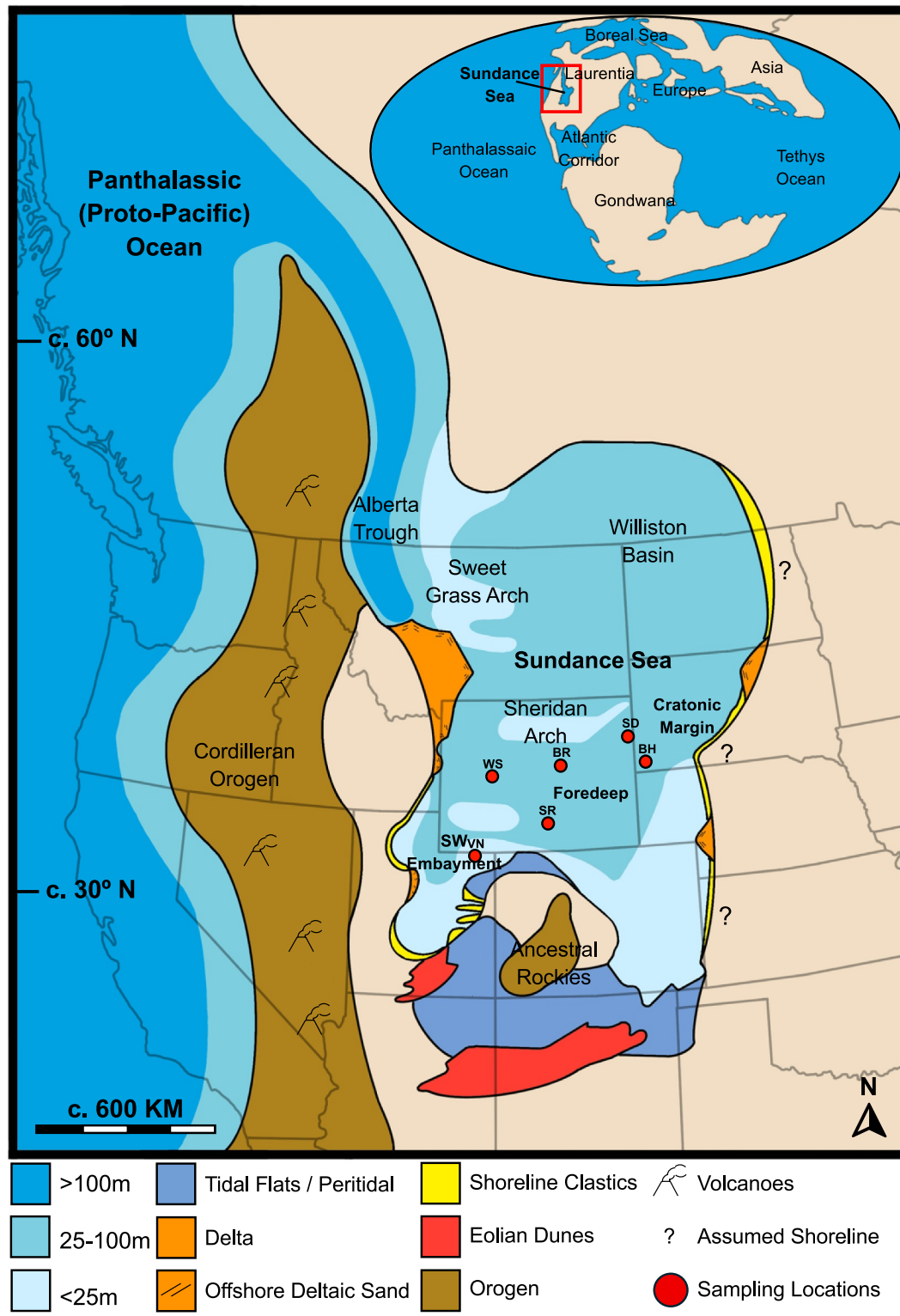

Figure 1. Sundance sea geography, Oxfordian. Adapted from Poulton (1984); Wroblewski and Morris (2022); and Schueth et al. (2025).

25724525, 2026, 7, Downloaded from https://agupubs.onlinelibrary.wiley.com/doi/10.1029/2025PA005364 by Open Research - University Of East Anglia , Wiley Online Library on [13/08/2026]. See the Terms and Conditions (https://onlinelibrary.wiley.com/terms-and-conditions) on Wiley Online Library for rules of use; OA articles are governed by the applicable Creative Commons License

25724525, 2026, 7, Downloaded from https://agupubs.onlinelibrary.wiley.com/doi/10.1029/2025PA005364 by Open Research - University Of East Anglia , Wiley Online Library on [13/08/2026]. See the Terms and Conditions (https://onlinelibrary.wiley.com/terms-and-conditions) on Wiley Online Library for rules of use; OA articles are governed by the applicable Creative Commons License

There are currently no direct quantitative paleotemperature estimates from North America for the Oxfordian (c. 161.5–154.8 Ma; International Commission on Stratigraphy, 2024) derived from clumped isotopes. Most existing studies rely on $\delta^{18}O$ and either target earlier intervals (e.g., Harris et al., 2017; Price et al., 2023, which focus on the Early to Middle Jurassic) or on later intervals (e.g., Gröcke et al., 2003; Husinec & Read, 2007; Wang et al., 2023, 2024, 2025, which focus on the Jurassic-Cretaceous boundary). Current estimates of paleotemperature in the Sundance Sea rely on carbonate $\delta^{18}O$ analyses, which require assumptions about the seawater $\delta^{18}O$ composition during carbonate precipitation (e.g., Danise et al., 2020). Given the semi-enclosed nature of the epicontinental seaway, with higher evaporation and freshwater input, seawater $\delta^{18}O$ was likely highly variable and not representative of open-ocean values (Macarewich et al., 2021), making paleotemperature reconstructions from this proxy inherently uncertain. For these reasons, the reported $\delta^{18}O$ values from the Sundance Sea are likely different from those from coeval open ocean and consequently result in unreliable paleo-sea temperatures. This gap in the record limits our ability to reconstruct North America's climatic evolution through the Jurassic, particularly in identifying potential maximum temperatures, their ecological impacts, and the causal relationship between pCO_2 and mid-latitude temperature during the Oxfordian. To address this gap, we present new carbonate clumped isotope (Δ_{47}) data from Oxfordian belemnite (*Pachyteuthis densus*) and *Gryphaea* (*Gryphaea nebraskensis*) fossils from the Oxfordian Redwater Shale Member of the Sundance Formation to constrain temperatures of the Sundance Sea more accurately, providing the first direct quantitative constraints on paleotemperature estimates based on clumped isotope analysis for this interval in North America.

Our reconstructed marine temperatures across the basin during the Oxfordian are based on Δ_{47} and were used alongside carbonate $\delta^{18}O$ analyses to calculate the first direct quantitative estimates of coeval seawater $\delta^{18}O$ ($\delta^{18}O_{SW}$). We used temporal trends in these temperatures within the wider Jurassic context to assess the existence of an Oxfordian Warm Interval. A three-stage screening process involving cathodoluminescence, elemental and stable isotope analyses was used to select fossilized carbonate material showing very limited diagenetic alteration, ensuring that the clumped isotope data are representative of the seawater in which the sampled organisms lived. $^{87}Sr/^{86}Sr$ analyses of the belemnites were also undertaken, allowing evaluation of the balance between open-ocean and terrestrially sourced waters in the Sundance Sea (McArthur et al., 2020).

1.2. Geological Context

During the Mid to Late Jurassic (Bajocian to Oxfordian), the Sundance Sea formed a shallow, elongate retro-arc foreland basin that extended south–east to north–west for nearly 2,000 km from southern Utah northward into Alberta and British Columbia (Figure 1). It was bounded to the west by the highlands of the Cordilleran volcanic arc and to the east by the North American craton. Most reconstructions depict the seaway with a single, narrow entrance in its north–west linking it to the Panthalassic (Proto-Pacific) Ocean (Schueth et al., 2025; Wroblewski & Morris, 2022). The basin reached a maximum depth of about 100 m toward its western margin (Kvale et al., 2001). Its narrow entrance, great length, and shallowness likely led to restricted circulation and the development of pronounced temperature and salinity gradients (Danise & Holland, 2018; McMullen et al., 2014; Tang & Bottjer, 1996). Mid to Late Jurassic sediments deposited in the Sundance Sea include a series of sandstones and shales belonging to the Gypsum Spring (Mid Jurassic) and Sundance (Late Jurassic) formations and lateral equivalents, including the Twin Creek and Stump Formations, respectively (Imlay, 1947; Uhlir et al., 1988; Massare et al., 2013; (Figure 2)). These deposits record a series of marine transgressions and regressions that span the Bathonian to Oxfordian (c. 168.2–154.8 Ma; Imlay, 1980). These are underlain unconformably by the Triassic Chugwater Group (Imlay, 1947) and overlain by the Late Jurassic terrestrial-dominated Morrison Formation (Kvale et al., 2004; Massare et al., 2013). This transition from marine to terrestrial sedimentation reflects the progressive infilling of the basin coincident with tectonic uplift in the Cordilleran fold belt and an associated increase in erosion (Brenner & Davies, 1974).

In Wyoming, and adjacent areas of Utah and North Dakota, there is local variability in the conventional lithostratigraphic nomenclature of the deposits of the Sundance Sea, which largely reflects lateral facies changes, particularly at the margins of the former seaway. This contrasts with consistent basin-scale unconformities or depositional hiatuses that separate the laterally variable marine deposits (Figure 2), interpreted as third-order (c. 0.5–3 Ma duration) transgressive-regressive sequences (e.g., Danise & Holland, 2018).

This study focuses on the Redwater Shale Member of the Sundance Formation and its lateral equivalent(s) (Redwater Member, Stump Formation; (Figure 2)), which are bounded by the unconformities conventionally

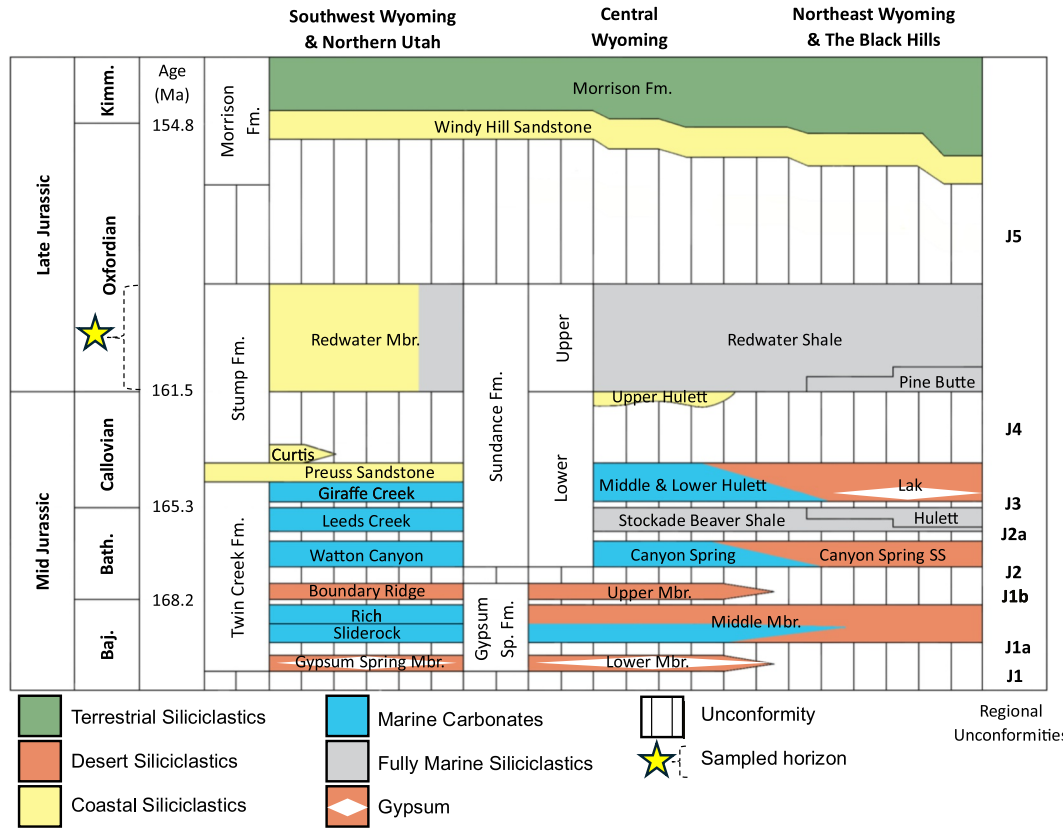

Figure 2. Chronostratigraphic and sequence stratigraphic framework of the Study Area–Utah to the Black Hills. Adapted from Neely (1937); Imlay (1947); Pipiringos and O'Sullivan (1978); Danise and Holland (2018); Danise et al. (2020).

termed J4 and J5 (Pipiringos & O'Sullivan, 1978). The Redwater Shale Member records the largest and final major Jurassic marine incursion in North America. The member is up to 30 m thick (Imlay, 1947; Pipiringos, 1968). In general, it is a medium to dark grey, glauconitic shale, indicative of offshore suspension settling over a broad area (e.g., Danise & Holland, 2018; McCullen et al., 2014). In places, thin, laterally discontinuous beds of glauconitic sandstone, and poorly indurated shelly limestones (coquinas) comprised mainly of bivalves (including *Ostrea* or *Gryphaea*), and belemnites (Imlay, 1947; Uhlir et al., 1988) may represent offshore storm beds (e.g., Danise & Holland, 2018; McCullen et al., 2014). In central Wyoming, the member is characterized by thinly bedded green-grey, glauconitic cross-bedded sandstone and abundantly bioturbated tan to olive-green fine sandstone, which Massare et al. (2013) interpret as an isolated shallow-water wave-dominated siliciclastic shelf or platform. Based on ammonite assemblages, the lower part of the member has been correlated with the Oxfordian *Cardioceras cordatum* Zone (Imlay, 1982). Ammonites and other fauna typically associated with the late Oxfordian have not been found in the Redwater Shale Member, nor in any of its lateral equivalents, which extend into the Western Interior of the United States, as far as the Pryor Mountains, Montana (Arkell, 1956; Imlay, 1947, 1980; Reeside, 1919). Reeside (1919) and Pipiringos (1957) explicitly assigned the Redwater Shale Member to the Early Oxfordian and the *Cardioceras cordatum* Zone because it is characterized by uninterrupted deposition within the sequence, and the only ammonites found across the basin are Early Oxfordian in age.

A unit stratigraphically higher than the Redwater Shale Member, termed the Windy Hill Sandstone, was traditionally assigned to the Sundance Formation based on its marine-brackish fauna (Pipiringos & O'Sullivan, 1978). However, the unit is unconformable (J5) with the Redwater Shale Member and interfingers with the base of the Morrison Formation. Consequently, it has since been reassigned to the Morrison Formation (Peterson, 1994; USGS, 2025) but remains in the Oxfordian (Kowallis et al., 1998; USGS, 2025).

In this study, the Redwater Shale was characterized as glauconitic shale at all outcrops, with no significant variation in lithology, making it relatively uniform. Belemnites are present both in abundant distinct horizons and

25724525, 2026, 7, Downloaded from https://agupubs.onlinelibrary.wiley.com/doi/10.1029/2025PA005364 by Open Research - University Of East Anglia , Wiley Online Library on [13/08/2026]. See the Terms and Conditions (https://onlinelibrary.wiley.com/terms-and-conditions) on Wiley Online Library for rules of use; OA articles are governed by the applicable Creative Commons License

as isolated individuals throughout the member. Bivalves (mainly *Gryphaea* and *Ostrea*) are more sparsely distributed and occur only as isolated individuals.

2. Materials and Methods

2.1. Sample Collection

Fossilized belemnite rostra and *Gryphaea* valves were collected from outcrops of the Redwater Shale Member at six locations across the states of Wyoming, Utah, and South Dakota (Figure 1). Species identification was conducted based on their gross morphology. The nature and uniformity of the outcrops, as well as the belemnite samples occurring on weathering surfaces, made it difficult to constrain them stratigraphically within the Redwater Shale. Therefore, the data generated in this study represent averaged values, along with range and distribution statistics, for the Redwater Shale Member.

2.2. Sample Preparation

Sample powders were micro-drilled from multiple well-preserved areas of each fossil. These powders were mixed to generate a homogenized average sample for each fossil and divided into aliquots for subsequent geochemical analyses.

2.3. Cathodoluminescence

Thin sections were prepared from belemnite and *Gryphaea* samples used in this study to examine their morphology and make an initial assessment of their state of preservation using cathodoluminescence (CL). The fossils were imaged using a CL8200MK 5-2 Optical CL System (CITL) with an accelerating voltage of 24 kV and a beam current of 350–400 mA. Areas that showed strong luminescence indicative of diagenetic alteration, including the alveolus, exterior, and apical regions of the belemnites, as well as observable cracks and fractures in both the belemnites and *Gryphaea*, were avoided for further sampling. Overall, <20% of the belemnite thin sections luminesced. Only non-luminescent (unaltered) areas were sampled and crushed to a fine powder (<60 μm) for elemental and isotopic analysis.

2.4. Optical Emission Spectrometry

For elemental analysis, 4.5 mg (±0.5 mg) aliquots of the crushed powder were digested in 2% HNO_3 and analyzed for selected elemental abundances using a Thermo iCAP 7000 Inductively Coupled Plasma Optical Emission Spectrometer (ICP-OES) at the University of Plymouth. The reproducibility of the measured concentrations for each element in procedural duplicates (RSB and RSB2) was better than ±3% of the total range measured across all aliquots. All repeat analyses of the standard reference material, JLS-1 (n = 8), were within 2% of the certified values for Sr, Mn, Ca, and Mg, and within 10% for Fe. Elemental concentrations were used as a secondary screening tool to exclude diagenetically altered material from isotopic analyses, as well as to characterize the hydrographic morphology, environmental conditions, and processes operating in the Sundance Sea.

2.5. Stable Isotope Analysis

For carbon and oxygen stable isotope analysis, 120 μg (±5 μg) of crushed powder was loaded into a heated block at 72°C in a Gasbench II automatic gas preparation module linked to a Delta V Advantage continuous flow isotope ratio mass spectrometer via a ConFlo IV universal gas management interface at the University of Plymouth. The samples were flushed with helium to remove air before adding 105% H_3PO_4 to digest the powder for >60 min. The equilibrated CO_2 generated by sample digestion was sampled 10 times for 30 s. Calibration was conducted offline using data from international reference materials (NBS19, CO-8, and CO-9) and well-characterized in-house calcite standards (CAMPU and UPIS) run periodically alongside the samples, procedural duplicates (RSB and RSB2), and blanks. The standard deviation for repeated analyses of the reference materials, in-house standards, and procedural duplicates was <0.09‰ for $\delta^{13}C$ and <0.09‰ for $\delta^{18}O$.

2.6. Strontium Isotope Analysis

$^{87}Sr/^{86}Sr$ analysis employed the column chemistry methods outlined in Kramchaninov et al. (2012), and samples were analyzed using a Multi-Collector Inductively Coupled Plasma Mass Spectrometer (MC-ICP-MS) (Thermo-

25724525, 2026, 7, Downloaded from https://agupubs.onlinelibrary.wiley.com/doi/10.1029/2025PA005364 by Open Research - University Of East Anglia , Wiley Online Library on [13/08/2026]. See the Terms and Conditions (https://onlinelibrary.wiley.com/terms-and-conditions) on Wiley Online Library for rules of use; OA articles are governed by the applicable Creative Commons License

Finnigan Neptune MC-ICP-MS) at the University of Durham. Strontium extracted from 1 mg of sample powder was run 50 times using an extended integration time of 8 s to ensure greater ion collection during each run, following approaches similar to those of Gerritzen et al. (2024) and Zhou et al. (2020). As a result, the internal precision achieved for the $^{87}Sr/^{86}Sr$ ratio was 3.2×10^{-6} (2SD). To normalize results, samples were analyzed alongside IAPSO (modern seawater), which yielded a measured $^{87}Sr/^{86}Sr$ ratio of $0.7091734 \pm 2.7 \times 10^{-6}$ in line with the published $^{87}Sr/^{86}Sr$ ratio of $0.7091790 \pm 5.0 \times 10^{-6}$ (El Meknassi et al., 2020), and corrected using NBS987, yielding 0.7102510 ($\pm 7.0 \times 10^{-6}$ 2SD, $n = 9$).

2.7. Clumped Isotope Analysis

Δ_{47} clumped isotope analysis was performed on 4 mg aliquots of carbonate powder, split from a homogenized sample. The aliquots were reacted for 30 min at 87°C with 107% H_3PO_4 in a common acid bath (3–4 replicates) following the methods of Paxton et al. (2023). The resulting purified CO_2 samples were then analyzed using a dual-inlet Multi-Isotopologue Ratio Analyzer (University of East Anglia (UEA)). The standard deviation for repeated analyses of 60–80 cycles of sample-reference gas over 2 hr was <0.008‰. To maintain Δ_{47} standardization, raw Δ_{47} data, named Δ_{47}(LRF) (Local Reference Frame), were converted to the Intercarb-Carbon Dioxide Equilibrium Scale (I-CDES) (Bernasconi et al., 2021) to ensure that the reported data were comparable between laboratories (Dennis et al., 2018). To convert from the local reference frame derived from temperature reactions at 87° to 90°C, an acid fractionation factor of 0.003% (experimentally determined at UEA and in agreement with the theoretical fractionation determined by Guo et al. (2009)) was subtracted from the transfer functions. Carbonate standards ETH1, ETH3, and an internal standard, UEA Carrara Marble (UEACMST), were measured daily during analysis, typically 1 standard for every three samples (Tables ST5 and ST6), to estimate long-term measurement uncertainty and to determine the transfer function between the local reference frame and I-CDES. Δ_{47} values used for ETH1 and ETH3 at 87°C acid digestion were empirically derived at UEA, 0.218‰ for ETH1 and 0.613‰ for ETH3. A subset of samples was also measured at ETH Zürich using a Thermo Fisher MAT253 coupled to a Kiel IV device, following the methods of Müller et al. (2017) and Looser et al. (2023). Each sample was measured 10 and 15 times across different runs using a 50:50 sample-to-standard ratio. Normalization to the I-CDES scale was accomplished using the ETH1, ETH2, and ETH3 standards (Bernasconi et al., 2021).

3. Results

3.1. Diagenesis Screening

Optical assessment of the belemnite rostra showed that all selected samples were translucent and honey-colored and, along with the *Gryphaea* valves, showed no visible signs of warping or shearing, indicative of unaltered calcite (Price, Baker, et al., 2016; Price, Főzy, & Pálfy, 2016). CL revealed localized calcite diagenetic alteration, particularly along the outer margins, apical lines, and major growth bands of the belemnites (smaller growth lines did not show diagenetic alteration). These altered areas show as bright orange, indicating the likely presence of Mn^{2+} (Barbin, 1995; Ullmann & Korte, 2015). As noted above, these areas were excluded during sub-sampling. Areas of unaltered calcite are non-luminous or display as a dark blue (Barbin, 1995; Ullmann & Korte, 2015). Based on the ICP-OES criteria outlined by Danise et al. (2020) and corrected to a calibration 37.5 wt% Ca in mollusk $CaCO_3$ (Hoffmann & Stevens, 2019; Suzuki & Nagasawa, 2013) (i.e., Fe < 0.5 mmol/mol, Mn < 0.2 mmol/mol, Sr > 1 mmol/mol in belemnites, and Sr > 0.75 mmol/mol in bivalves), all analyzed belemnites and *Gryphaea* demonstrated very good preservation. Isotope analyses yielded $\delta^{13}C_{(VPDB)}$ and $\delta^{18}O_{(VPDB)}$ values within the expected ranges for well-preserved belemnites and bivalves. $\delta^{13}C$ values ranged between 0.84‰ and 3.50‰ for belemnites and $\delta^{13}C$ values between 6.00‰ and 6.33‰ for *Gryphaea*. $\delta^{18}O$ values between −3.73‰ and −0.36‰ in both taxon (Figure 3). Expected Jurassic marine biogenic carbonate data were compiled for samples that had passed preservation criteria applied in the original studies. The complete data set from this study is available in Data Set S1, https://doi.org/10.24382/1d114a19-9d2f-4cc7-80dd-3a61db8910d6, and the data sets used for the range of stable isotopes can be found in ST8. The Redwater Shale Member at studied localities produced well-preserved belemnites and *Gryphaea* suitable for stable isotope analysis (cf. Danise et al., 2020). Of the 144 belemnites and *Gryphaea* initially screened, many did not meet the higher diagenetic threshold described above for clumped isotope analysis.

25724525, 2026, 7, Downloaded from https://agupubs.onlinelibrary.wiley.com/doi/10.1029/2025PA005364 by Open Research - University Of East Anglia , Wiley Online Library on [13/08/2026]. See the Terms and Conditions (https://onlinelibrary.wiley.com/terms-and-conditions) on Wiley Online Library for rules of use; OA articles are governed by the applicable Creative Commons License

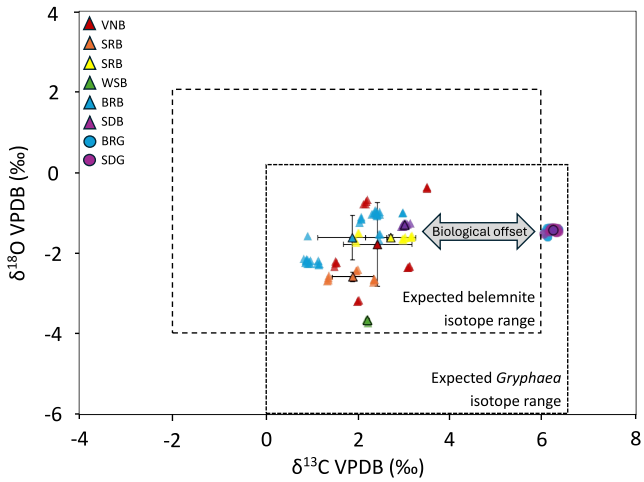

Figure 3. Sundance Sea $\delta^{13}C$ and $\delta^{18}O$ belemnite and *Gryphaea* results (analysis conducted at University of Plymouth, University of East Anglia, and ETH Zürich) and the expected range of unaltered calcite in both taxa calculated from published Jurassic data sets (see ST8 for published Jurassic isotopes). Shaded points are individual samples with the main block and errors for the site average.

3.2. Strontium Isotope Ratios

The $^{87}Sr/^{86}Sr$ ratio composition of seawater is controlled by inputs from multiple sources, dominated by radiogenic continental runoff ($^{87}Sr/^{86}Sr \sim 0.711$) and unradiogenic mantle-derived submarine hydrothermal fluids ($^{87}Sr/^{86}Sr \sim 0.703$). The balance between these sources changes in a well-documented manner throughout geological time, as shown by the seawater $^{87}Sr/^{86}Sr$ record compiled by McArthur et al. (2020). Consequently, the age of marine carbonates can be estimated by comparing their $^{87}Sr/^{86}Sr$ ratio with a calibration curve for this record. Furthermore, given age constraints, deviations from this curve can be used to identify differences in the balance between radiogenic and unradiogenic strontium, which potentially indicate source contributions. Our $^{87}Sr/^{86}Sr$ data show that the Sundance Basin has an average ratio of 0.7068620 ($\pm 1.4 \times 10^{-5}$ 1SE, $n = 21$). There are differences between the averages for the foredeep, with a ratio of 0.7068410 ($\pm 5.2 \times 10^{-6}$ 1SE, $n = 7$); cratonic margin, with a ratio of 0.7068500 ($\pm 5.5 \times 10^{-6}$ 1SE, $n = 6$); the southwestern embayment, with a ratio of 0.7068380 ($\pm 1.2 \times 10^{-5}$ 1SE, $n = 4$); and the southern shoreline, with a ratio of 0.7068770 ($\pm 4.4 \times 10^{-6}$ 1SE, $n = 3$). The range of $^{87}Sr/^{86}Sr$ values, when compared with the global $^{87}Sr/^{86}Sr$ curve, gives an age range that extends from the early Oxfordian into the Kimmeridgian (Figure 4), with several samples plotting within the range of $^{87}Sr/^{86}Sr$ ratios expected in the Windy Hill Sandstone and the Morrison Formation (Figure 2), both of which are lithologically different from the Redwater Shale Member. All samples in this study were collected from the Redwater Shale Member, which has been correlated with the *Cardioceras cordatum* Zone (Imlay, 1982) and is therefore of Early Oxfordian in age. The absence of Late Oxfordian fauna further suggests that it is no younger than Mid-Oxfordian. It is more

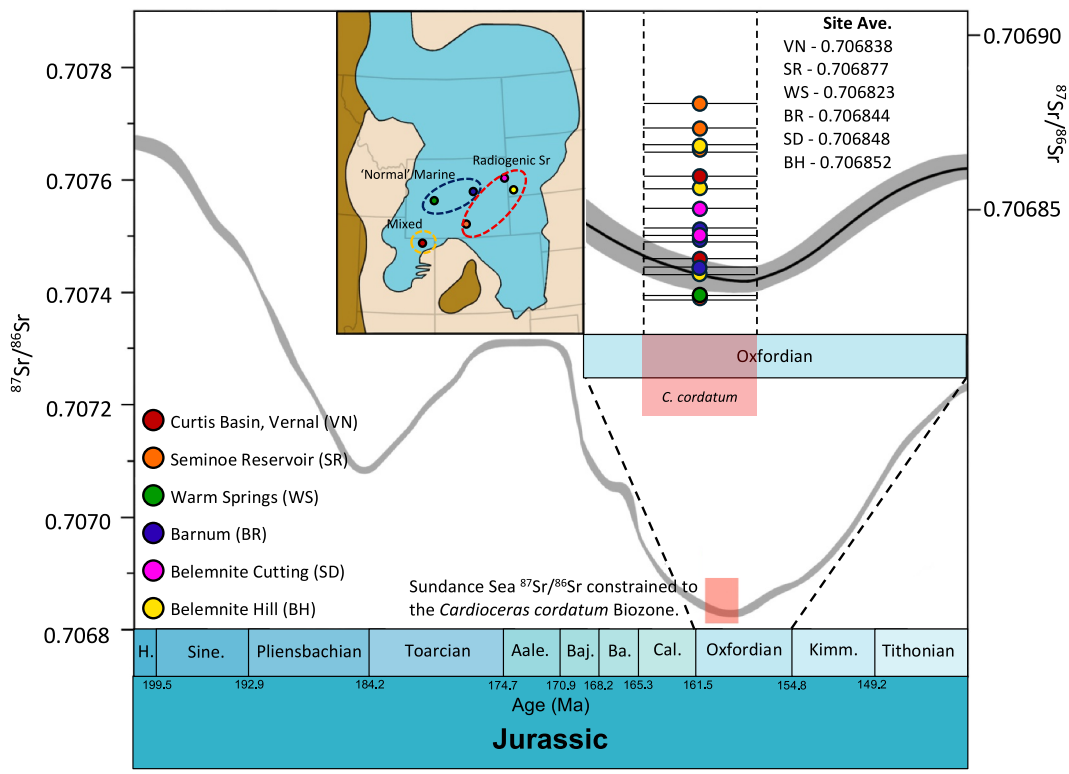

Figure 4. Sundance Sea $^{87}Sr/^{86}Sr$ Results (this study) plotted against the Global $^{87}Sr/^{86}Sr$ curve during the Jurassic with 95% confidence interval (the latter adapted from McArthur et al., 2020; Wierzbowski et al., 2017). Results are plotted in the *Cardioceras cordatum* biozone of the Sundance Formation.

25724525, 2026, 7, Downloaded from https://agupubs.onlinelibrary.wiley.com/doi/10.1029/2025PA005364 by Open Research - University Of East Anglia , Wiley Online Library on [13/08/2026]. See the Terms and Conditions (https://onlinelibrary.wiley.com/terms-and-conditions) on Wiley Online Library for rules of use; OA articles are governed by the applicable Creative Commons License

25724525, 2026, 7, Downloaded from https://agupubs.onlinelibrary.wiley.com/doi/10.1029/2025PA005364 by Open Research - University Of East Anglia , Wiley Online Library on [13/08/2026]. See the Terms and Conditions (https://onlinelibrary.wiley.com/terms-and-conditions) on Wiley Online Library for rules of use; OA articles are governed by the applicable Creative Commons License

likely, then, that the variation in $^{87}Sr/^{86}Sr$ values reflects variable amounts of radiogenic enrichment, and that the offset from the global $^{87}Sr/^{86}Sr$ curve is a result of freshwater runoff into the basin and proportionately reduced exchange with the open ocean during times of marine regression. However, we cannot exclude the possibility that minor alteration or inter-laboratory bias may affect the comparability of the records.

Following our preferred interpretation of a geological significance for the observed offset, the Southern Shoreline shows the highest radiogenic enrichment and the narrowest range of $^{87}Sr/^{86}Sr$ values (1.5×10^{-5}), reflecting significant freshwater input from the Ancestral Rockies and limited influence from variations in open-ocean exchange associated with marine transgression and regression. The SW Embayment and the Foredeep show similar, but lower radiogenic enrichment, indicating proportionately higher levels of marine input than the Southern Shoreline. The Cratonic Margin shows intermediate radiogenic enrichment, reflecting freshwater input (from the North American Craton) that was proportionately higher than in the SW Embayment and Foredeep but lower than in the Southern Shoreline. Despite these average differences, the SW Embayment, Foredeep, and Cratonic Margin all show a similar range of $^{87}Sr/^{86}Sr$ values (3.9×10^{-5}, 3.8×10^{-5}, and 4.0×10^{-5}, respectively), suggesting that these regions were similarly susceptible to variations in open-ocean exchange associated with marine transgression and regression.

3.3. Δ_{47} Derived Temperatures

Clumped isotopes are a valuable tool for temperature reconstructions because they do not rely on a preconceived isotopic composition of the seawater in which the calcite precipitated (Ghosh et al., 2008; Price et al., 2020). This composition is generally considered representative of the coeval global average for open ocean, but may differ substantially from the average seawater composition in marginal settings, particularly in restricted basins where exchange with the open ocean is limited. Clumped isotopes do, however, rely on stringent burial temperature constraints because at high temperatures, the bonds between ^{13}C and ^{18}O isotopes in carbonate lattices are susceptible to solid-state re-ordering, resulting in higher Δ_{47} derived temperatures. Consequently, both the diagenetic history and more traditional geochemical screening techniques for carbonate recrystallization (Section 3.1) must be considered in deep time Δ_{47} paleothermometry (Hemingway & Henkes, 2021; Henkes et al., 2018; Looser et al., 2023; Passey & Henkes, 2012).

It is likely that the Jurassic sediments deposited in the Sundance Sea were variably buried and uplifted to varying depths during the Laramide orogenic cycle (40–80 Ma) (Fan & Carrapa, 2014; Stevens et al., 2016) and thus experienced elevated temperatures. Diffusion of carbon and oxygen isotopes within the carbonate mineral lattice may reset the initial bond-ordering and initiate recrystallization (e.g., Henkes et al., 2018). However, inferred burial history data for the Stump and Sundance formations (e.g., Gottardi et al., 2019) suggest that the Sundance sediments were typically buried to depths of no more than 2–3 km, and therefore were unlikely to have seen temperatures high enough for bond-reordering. Geothermal gradients in foreland basins typically range from 15° to 25°C/km (Allen & Allen, 2013), so at an assumed surface temperature of 25°C, the maximum temperature possible at 3 km would have been c. 100°C. Theoretical calculations based on laboratory experiments generally provide evidence that solid-state diffusion, even under wet and high-pressure conditions, is negligible below 100°C burial temperatures on a timescale of 100–160 Ma (Hemingway & Henkes, 2021). Looser et al. (2023), however, identified that belemnite calcite is more susceptible to bond reordering in clumped isotopes at lower temperatures. Using the kinetic parameters of Looser et al. (2023) and the model of Hemingway and Henkes (2021), together with the calculated burial depth and duration, suggests that partial bond reordering of up to 10% is possible for at least some of the Sundance belemnites. Thus, it is assumed that the belemnite rostra analyzed in this study were only marginally recrystallized during diagenesis, and the calculated temperatures for the Sundance Sea presented here may therefore be up to 3°C warmer (Table 1).

To evaluate Jurassic marine temperatures, Equation 1, developed by N. T. Anderson et al. (2021), was employed to calculate $t\Delta_{47}$. It was selected for its broad temperature calibration range (0.5°–1,100°C) and extensive inter-laboratory use.

$$t\Delta_{47} = \left(\frac{\left(0.0391 \pm 0.0004 * 10^{6}\right)^{0.5}}{\Delta_{47}\text{I-CDES} - 0.154 \pm 0.004} \right) - 273 \quad (1)$$

Paleoceanography and Paleoclimatology

10.1029/2025PA005364

Table 1
Stable and Clumped Isotopic Data Derived From Belemnite (Pachyteuthis densus) and Gryphaea (Gryphaea nebrascensis)

Sample ID	Location	Species	*n*	$\delta^{13}C$ VPDB (‰)	$\delta^{18}O_{Carb}$ VPDB (‰)	$\delta^{18}O_{Carb}$ VSMOW (‰)	Δ_{47} I-CDES	Reported Δ_{47} Temp (°C)	Adjusted for maximum reordered Δ_{47} Temp (°C)	1SE	$\delta^{18}O_{SW}$ VSMOW (‰)	1SE	$^{87}Sr/^{86}Sr$
VNB4	Vernal, UT	*P. densus*	4	3.10	−2.35	28.44	0.589	26.7	23.7	6.0	−2.7	1.4	0.706832
VNB10	Vernal, UT	*P. densus*	4	3.12	−2.25	28.54	0.597	23.8	20.8	6.6	−3.2	1.5	0.706822
VNB11	Vernal, UT	*P. densus*	3	3.50	−0.37	30.47	0.552	40.3	37.3	5.1	2.2	1.1	n/a
VNB14	Vernal, UT	*P. densus*	3	2.01	−3.18	27.58	0.637	11.3	8.3	1.6	−7.1	0.4	n/a
VNB18	Vernal, UT	*P. densus*	4	2.18	−0.74	30.10	0.587	27.5	24.5	1.9	−0.9	0.4	0.706861
SRB13	Seminoe Reservoir, WY	*P. densus*	4	1.37	−2.63	28.15	0.566	35.0	32.0	4.2	−1.3	0.9	0.706884
SRB17	Seminoe Reservoir, WY	*P. densus*	3	1.98	−2.42	28.36	0.579	30.2	27.2	3.8	−2.0	0.8	0.706878
SRB33	Seminoe Reservoir, WY	*P. densus*	4	2.36	−2.67	28.36	0.560	37.4	34.4	4.4	−0.7	0.9	0.706869
WSB5	Warm Springs, WY	*P. densus*	4	2.22	−3.67	40.70	0.565	35.4	32.4	1.7	−2.1	0.4	0.706823
BHB5	Edgemont, SD	*P. densus*	4	1.99	−1.61	29.21	0.571	33.0	30.0	3.5	−0.5	0.8	0.706870
BHB7	Edgemont, SD	*P. densus*	4	3.16	−1.59	29.22	0.576	31.3	28.3	6.6	−0.9	1.4	0.706856
BHB11	Edgemont, SD	*P. densus*	4	2.99	−1.63	29.18	0.549	41.8	38.8	4.4	1.3	0.9	0.706830
BRB7	Barnum, WY	*P. densus*	4	1.15	−2.09	28.70	0.585	27.9	24.9	2.9	−2.1	0.6	0.706843
BRB7 (Dup)	Barnum, WY	*P. densus*	11	0.92	−2.23	28.62	0.575	31.5	28.5	3.0	−1.4	0.6	n/a
BRB24	Barnum, WY	*P. densus*	3	2.47	−2.16	33.50	0.581	29.3	26.3	2.1	−1.9	0.4	0.706840
BRB28	Barnum, WY	*P. densus*	4	2.07	−1.58	29.23	0.589	26.5	23.5	7.2	−1.9	1.6	0.706832
BRB44	Barnum, WY	*P. densus*	3	2.97	−1.13	29.69	0.578	30.5	27.5	2.6	−0.6	0.6	0.706832
BRB44 (Dup)	Barnum, WY	*P. densus*	15	2.42	−1.02	29.87	0.583	28.8	25.8	2.1	−0.8	0.5	n/a
BRG1	Barnum, WY	*G. nebrascensis*	11	6.17	−1.40	29.48	0.592	25.5	22.5	1.8	−1.9	0.8	0.706856
BRG2	Barnum, WY	*G. nebrascensis*	10	6.23	−1.46	29.42	0.574	32.1	29.1	1.8	−0.5	0.4	0.706861
SDB15	Sundance, WY	*P. densus*	11	3.01	−1.30	29.58	0.584	28.5	25.5	2.1	−1.1	0.5	0.706841
SDG5	Sundance, WY	*G. nebrascensis*	12	6.18	−1.40	29.48	0.576	31.1	28.1	4.0	−0.7	0.9	0.706851
SDG6	Sundance, WY	*G. nebrascensis*	14	6.24	−1.44	29.44	0.556	38.8	35.8	3.4	0.9	0.7	0.706851

Note. Samples from the Redwater Shale Member.

25724525, 2026, 7, Downloaded from https://agupubs.onlinelibrary.wiley.com/doi/10.1029/2025PA005364 by Open Research - University Of East Anglia , Wiley Online Library on [13/08/2026]. See the Terms and Conditions (https://onlinelibrary.wiley.com/terms-and-conditions) on Wiley Online Library for rules of use; OA articles are governed by the applicable Creative Commons License

25724525, 2026, 7, Downloaded from https://agupubs.onlinelibrary.wiley.com/doi/10.1029/2025PA005364 by Open Research - University Of East Anglia , Wiley Online Library on [13/08/2026]. See the Terms and Conditions (https://onlinelibrary.wiley.com/terms-and-conditions) on Wiley Online Library for rules of use; OA articles are governed by the applicable Creative Commons License

where Δ_{47} I-CDES is Δ_{47} converted from the local reference frame of the UEA laboratory to the international I-CDES scale (Section 2.7).

Across all facies and taxa (17 belemnites and 4 *Gryphaea* from 6 locations (Table 1)), Δ_{47} I-CDES analyses for the Sundance Basin during the Oxfordian ranged from 0.552‰ to 0.597‰ (sample aliquot average), corresponding to reconstructed temperatures ranging from 25.9° to 35.3°C. The overall mean temperature was 30.6°C (±1.6 1SE, $n = 23$) when calculated using the site averages. These results are consistent with similar Early and Mid-Jurassic warm intervals in China (Jin et al., 2024; Xianghui et al., 2020) and comparable with the Cretaceous Thermal Maximum (M. M. Jones et al., 2022). To confirm inter-laboratory validation, the Δ_{47} I-CDES of two samples (BRB7 and BRB44) were re-examined at the stable isotope facilities of both UEA and ETH Zürich, using different methods. They displayed a difference of 3.6°C ± 4.2 reported 1SE (27.9°C, 2.9 1SE over 4 aliquots, and 31.5°C, 3.0 1SE over 11 aliquots) and 1.7°C ± 3.3 reported 1SE (30.5°C, 2.6 1SE over 3 aliquots and 28.8°C, 2.1 1SE over 15 aliquots), respectively, and are within error at the 1SE level (Table 1). This demonstrates that the different methods yield closely consistent results, thereby supporting the validity of the reconstructed temperature values.

Our data (Figure 5 and Table 1) indicate a temperature difference between the foredeep (Barnum, Warm Springs), the cratonic margin (Belemnite Cutting, Sundance, and Belemnite Hill, Edgemont), and the shallowing southwestern embayment (Curtis Basin, Vernal), 31.9°C (±1.3 1SE, $n = 15$) versus 25.9°C (±1.5 1SE, $n = 5$). Furthermore, Barnum, situated in the foredeep, had a lower temperature than areas closer to the shoreline (Seminoe Reservoir), 29.0°C (±0.8 1SE, $n = 8$) versus 34.1°C (±1.3 1SE, $n = 3$).

3.4. $\delta^{18}O$ Seawater Values

Equation 2, derived from data from Kele et al. (2015), was used to calculate $\delta^{18}O_{SW}$

$$\delta^{18}O_{SW} = \frac{\left(1000 + \delta^{18}O_{Carb(VSMOW)}\right)}{\exp\left(\frac{20 * 1000}{t\Delta_{47} - 273.15} - 36\right)/1000} - 1000 \quad (2)$$

where $\delta^{18}O_{Carb\ (VSMOW)}$ is the oxygen isotopic composition of the belemnite rostra and *Gryphaea* valves (vs. VSMOW), and $t\Delta_{47}$ is the temperature derived from clumped isotope analysis.

The equation of Kele et al. (2015) was selected because it best represents oxygen isotope fractionation in mollusks. Other paleotemperature equations (c.f., F. A. Anderson & Arthur, 1983) typically yield higher temperature estimates. Clumped isotope analyses of well-preserved aragonite phragmocones and calcite rostra of belemnites (Vickers et al., 2021) demonstrate that applying the Kele et al. (2015) calibration to calcite yields calculated oxygen isotope compositions of seawater similar to those of aragonite and, therefore, provides the most reliable temperature reconstructions. The calculated Sundance Sea $\delta^{18}O_{sw}$ ranges from −2.3‰ (±1.5 1SE, $n = 5$) to −0.1‰ (±0.7 1SE, $n = 3$). The most southern site (Curtis Basin, Vernal), corresponding to the southwestern embayment, exhibits the lowest value of −2.3‰ (±1.5 1SE, $n = 5$). The Sundance Sea's foredeep site (Barnum) is higher in $\delta^{18}O_{sw}$ at −1.4‰ (±0.2 1SE, $n = 8$) as compared with sites closer to its shoreline in the Southwest Embayment and Warm Springs, −2.1‰ (±0.4 1SE, $n = 1$). These are both lower than the $\delta^{18}O_{sw}$ from sites in the cratonic margin −0.1‰ (±0.7 1SE, $n = 3$) for Belemnite Hill, Edgemont and −0.2‰ (±0.4 1SE, $n = 6$) when averaged with Belemnite Cutting, Sundance, farther east. Across all data sites, the Sundance Sea has an average of −1.3‰ (±0.4 1SE calculated from specimen average, $n = 23$) based on the corresponding $t\Delta_{47}$. This is similar in value to present-day high latitude (70°–90°) (Le Grande & Schmidt, 2006). The two specimens yielding extreme temperatures of 40° and 11°C from the Curtis Basin, Vernal (VNB11 and VNB14), resulted in calculated $\delta^{18}O_{sw}$ values of 2.2‰ and −7.1‰, respectively, and account for the high uncertainty reported for the Curtis Basin, Vernal. The cause of these anomalous values is not apparent but appears temperature driven, not an alteration in $\delta^{18}O_{Carb}$, which falls within expected values (Figure 3). This discrepancy may reflect an analytical uncertainty, a statistical artifact, or an unrecognized diagenetic effect. Although the underlying cause remains uncertain, it highlights the importance of analyzing multiple samples from a single horizon when conducting clumped isotope analysis.

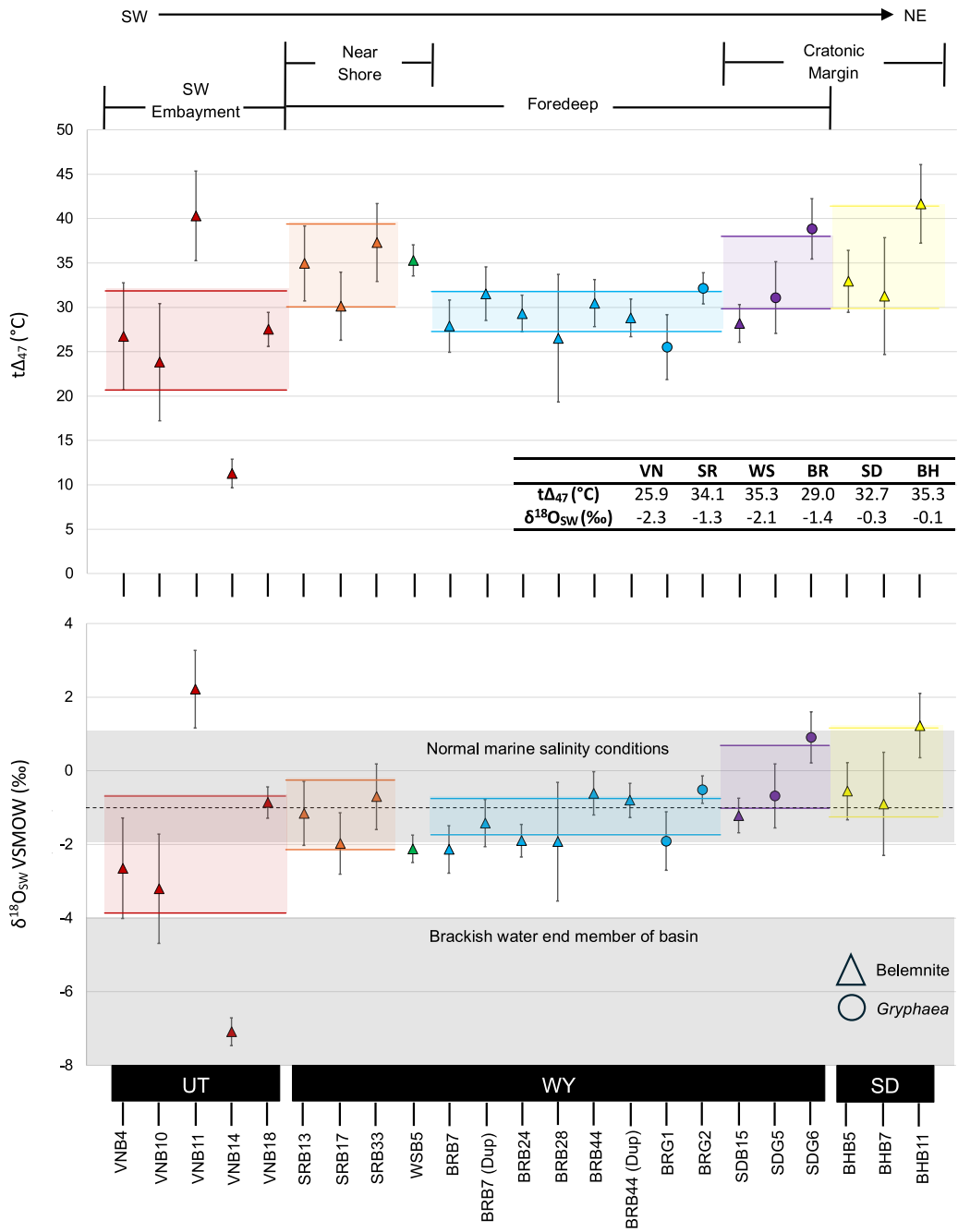

	VN	SR	WS	BR	SD	BH
$t\Delta_{47}$ (°C)	25.9	34.1	35.3	29.0	32.7	35.3
$\delta^{18}O_{SW}$ (‰)	-2.3	-1.3	-2.1	-1.4	-0.3	-0.1

Figure 5. $t\Delta_{47}$ (Top) and $\delta^{18}O_{SW}$ [Bottom] measured from Oxfordian belemnites and *Gryphaea* from the Sundance Sea. Shading displays 95% confidence intervals from the site average. Error bars represent 1SE. The dotted line represents the Jurassic open ocean global average of $\delta^{18}O_{SW}$ at −1‰. Stated values in the table are site averages. Open ocean and brackish values derived from Le Grande and Schmidt (2006).

4. Discussion

4.1. Late Jurassic Marine Temperatures of North America

Our Δ_{47}-derived temperatures for the Oxfordian Sundance Sea, with site averages ranging from 25.9° to 35.3°C (22.9°–32.3°C when subject to maximum bond reordering), are higher than temperatures reconstructed using

25724525, 2026, 7, Downloaded from https://agupubs.onlinelibrary.wiley.com/doi/10.1029/2025PA005364 by Open Research - University Of East Anglia , Wiley Online Library on [13/08/2026]. See the Terms and Conditions (https://onlinelibrary.wiley.com/terms-and-conditions) on Wiley Online Library for rules of use; OA articles are governed by the applicable Creative Commons License

25724525, 2026, 7, Downloaded from https://agupubs.onlinelibrary.wiley.com/doi/10.1029/2025PA005364 by Open Research - University Of East Anglia , Wiley Online Library on [13/08/2026]. See the Terms and Conditions (https://onlinelibrary.wiley.com/terms-and-conditions) on Wiley Online Library for rules of use; OA articles are governed by the applicable Creative Commons License

F. A. Anderson and Arthur (1983) oxygen isotope paleothermometer equation (10°–29°C, mean 18°C, assuming $\delta^{18}O_{SW} = -1‰_{(VSMOW)}$; Danise et al., 2020). Indeed, the upper temperatures are warmer than any other (non-diagenetic) clumped temperatures reported to date from high (e.g., Vickers et al., 2019, 2020) and mid (Wang et al., 2025) paleolatitudes. When compared with the recent study by Wang et al. (2025), which presents open ocean clumped temperature data from similar paleolatitudes (21.8°–29.3°C, mean 25.6°C), our data demonstrate the warmth of large epicontinental seaways. We hypothesize that the higher temperatures recorded are due to heat drawn from the surrounding terrestrial craton, and that the near-landlocked Sundance Sea may have exerted an ameliorating influence on the climate of the adjacent land areas. The seaway was likely warmer due to several factors, including reduced heat loss to the open ocean and restricted circulation. However, our average temperature estimates are not particularly well represented by recent climate models for the Oxfordian (Valdes et al., 2021), which suggest annual SSTs of 16°–22°C in North America.

4.2. The Oxfordian Warm Interval

The upper limits of our Sundance Sea temperature data exceed previous estimates of an Oxfordian warming pulse proposed by Dera et al. (2011) and Bodin et al. (2015). When temperatures are recalculated from published belemnite $\delta^{18}O_{Carb}$ values using the equation of Kele et al. (2015) (Equation 3), they are comparable to those of both the Toarcian Oceanic Anoxic Event, with temperatures in excess of c. 35°C assuming $\delta^{18}O_{SW}$ $-1‰_{(VSMOW)}$ [$<\delta^{18}O_{Carb}$ $-2.77‰_{(VPDB)}$] (Sælen et al., 1996), and the Mid-Cretaceous Thermal Maximum (KTM) of the Western Interior Seaway, where clumped isotope derived temperatures range from 28° to 34°C (excluding likely reordered isotopic species) (M. M. Jones et al., 2022) (Figure 6). Our Oxfordian data, together with these mid-Cretaceous values, are similar to those of the warmest modern tropical seas (M. M. Jones et al., 2022; Locarnini et al., 2019), emphasizing that the Oxfordian was a period of extreme warmth in North America's mid-latitudes.

$$t\delta^{18}O = \left(\frac{20 * 10^3}{10^3 \ln\left(\frac{1000 + \delta^{18}O_{carb(VSMOW)}}{1000 - 1}\right) + 36}\right) - 273.15 \quad (3)$$

where $t\delta^{18}O$ is the temperature in °C and $\delta^{18}O_{carb(VSMOW)}$ is the oxygen isotopic composition of the carbonate rostra or valve (vs. VSMOW).

The effect of this extreme warmth on the regional ecosystem is potentially significant and likely posed a high risk of marine ecosystem degradation due to reduced oxygen availability and heat stress, which affect ecosystem composition, functionality, and biodiversity (Keeling et al., 2010; Ullmann et al., 2014). Consequently, the elevated temperatures within the Sundance Sea could have compelled certain species to seek cooler environments and food sources or to migrate to areas that are either poleward or deeper. Specifically, some organisms, such as corals and radiolarians, have upper thermal limits of around 33°C, while the upper thermal limits for echinoderms, foraminifera, and cephalopods are marginally higher, at 35°C (Song et al., 2014). This is further supported by reduced diversity of marine vertebrates in the Sundance Sea compared with Europe at similar latitudes (Massare et al., 2013). Ostracods, gastropods, and bivalves were the most thermally tolerant groups, with some capable of surviving temperatures exceeding 40°C (Song et al., 2014). Such elevated temperatures could explain low diversity, high dominance assemblages of body fossils and trace fossils identified in the Sundance Sea (e.g., McMullen et al., 2014; Tang & Bottjer, 1996).

4.3. Sundance Basin Paleosalinity and Oceanography

By combining biogenic carbonate oxygen isotope measurements with our clumped temperature data and applying the modified equation of Kele et al. (2015) to calculate $\delta^{18}O_{SW}$, we find that all sites fall within the 95% confidence interval of the estimated $-1‰_{(VSMOW)}$ value for the open ocean average marine $\delta^{18}O_{SW}$ value for an ice-free interval (Shackleton & Kennett, 1975) (Figure 5). Accordingly, we interpret the Sundance Sea as having near-normal salinity. The Sundance Sea appears to have been heavily buffered by open ocean waters entering from the north. However, we suggest against using this value to approximate $\delta^{18}O_{SW}$ in traditional $t\delta^{18}O$ paleothermometry studies of unaltered carbonates from marine facies in the Sundance Sea, because the site-specific derived $\delta^{18}O_{SW}$ varies across the basin (i.e., a difference of 2.4‰ from the southwest embayment to the cratonic

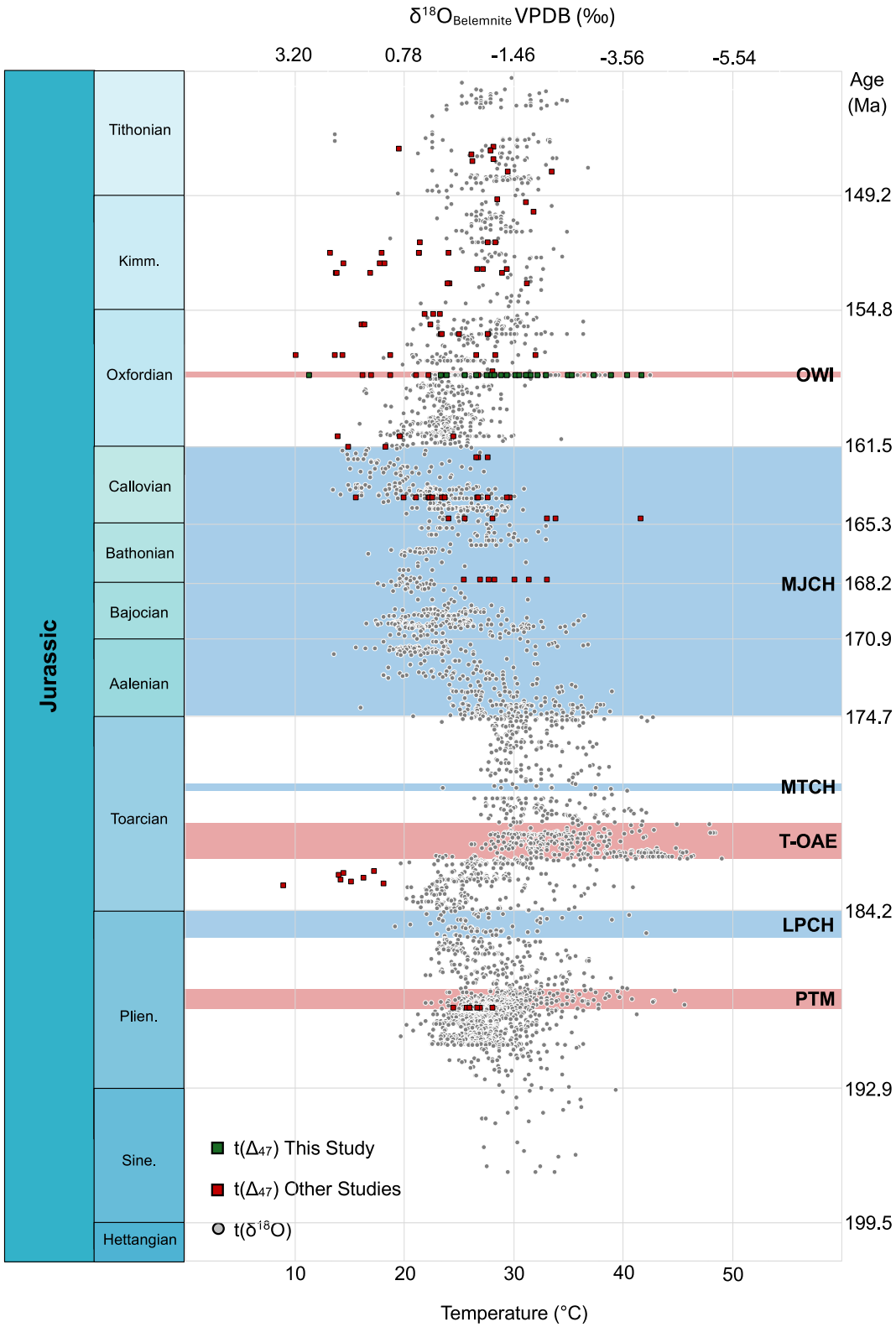

Figure 6.

25724525, 2026, 7, Downloaded from https://agupubs.onlinelibrary.wiley.com/doi/10.1029/2025PA005364 by Open Research - University Of East Anglia , Wiley Online Library on [13/08/2026]. See the Terms and Conditions (https://onlinelibrary.wiley.com/terms-and-conditions) on Wiley Online Library for rules of use; OA articles are governed by the applicable Creative Commons License

25724525, 2026, 7, Downloaded from https://agupubs.onlinelibrary.wiley.com/doi/10.1029/2025PA005364 by Open Research - University Of East Anglia , Wiley Online Library on [13/08/2026]. See the Terms and Conditions (https://onlinelibrary.wiley.com/terms-and-conditions) on Wiley Online Library for rules of use; OA articles are governed by the applicable Creative Commons License

margin). This is supported by research on other semi-isolated epeiric seas by Woodward et al. (2013), Scheiner et al. (2018), and Macarewich et al. (2021), who report heterogeneity in $\delta^{18}O_{sw}$ in these seaways due to high freshwater input, evaporation, and restricted water circulation. Similar patterns are observed in modern analogs of retro arc foreland basin seaways, such as the Persian Gulf, which exhibit temperature and isotopic variations between the cratonic margin and the orogenic front (Alosairi et al., 2011; Nesterov et al., 2021). Therefore, whenever possible, we recommend using a local $\delta^{18}O_{SW}$ value (e.g., where clumped isotope data are available) when interpreting $\delta^{18}O_{SW}$ in paleothermometry reconstructions ($t\delta^{18}O$) in ancient epeiric seaways. Based on currently available technology capabilities and the constraints of the geological record, obtaining more accurate estimates is likely to require a large number of measurements, as evident from the present study. These results further demonstrate that uncertainty in reconstructed regional $\delta^{18}O_{SW}$ values can contribute substantially to paleotemperature uncertainty, exceeding 10°C in some cases. Consequently, robust interpretation of some temperature estimates will require more tightly constrained regional $\delta^{18}O_{SW}$ reconstructions, highlighting an important avenue for future Jurassic paleoclimate research.

These Δ_{47} findings from the Sundance Sea are consistent with our Sr isotope analysis, which provides $^{87}Sr/^{86}Sr$ ratios indicative of an Oxfordian age when compared with biostratigraphic data (Imlay, 1982), but also reveals a pattern of radiogenic enrichment relative to the reconstructed global seawater curve (McArthur et al., 2020; Wierzbowski et al., 2018) when constrained to the Redwater Shale interval (c. 158 Ma). While the basin-average Δ_{47} findings fall within error of open ocean values, we interpret the slight enrichment in ^{87}Sr observed across the Sundance Sea as likely linked to the combined effects of high seawater temperatures, semi-restricted circulation, and continental weathering input (C. E. Jones, 2001; Pearce et al., 2015; Veizer, 1989). In warm, shallow epicontinental seas, limited circulation with the open ocean, elevated temperatures (resulting in increased evaporation), differences in bathymetry across the basin (foredeep vs. cratonic margin), and fluvial runoff can outpace the exchange of water from the open ocean. This restricted renewal of oceanic water likely prolonged the residence duration of dissolved elements, thereby amplifying local Sr isotope signals. As a result, even minor inputs of radiogenic Sr from fluvial runoff sourced from the adjacent continental craton could exert a stronger influence than they would in well-circulated open-ocean settings (i.e., Cochran et al., 2003; Curley et al., 2025), while the broadly buffered seaway maintains consistent ocean signals relative to the open ocean. The slightly elevated $^{87}Sr/^{86}Sr$ ratios observed in the Sundance Sea underscore the sensitivity of shallow epicontinental basins to temperature-modulated geochemical processes. This interpretation also supports our conclusions from $\delta^{18}O_{SW}$ that the Sundance Sea experienced marine to near-marine conditions.

The data, therefore, reflect a seaway approaching open marine conditions (cf. Cochran et al., 2003) at the foredeep sites despite their distance from the open ocean. However, the cratonic margin and southwestern embayment site deviate more in ocean chemistry, indicating either a disconnect from the deeper parts of the sea or an influx of fresh water into the basin from the southwest and east.

5. Conclusions

This study documents an Oxfordian Warm Interval, with seawater temperatures ranging from 28° to 35°C (25°–32°C if subject to maximum bond reordering). Δ_{47} analysis of well-preserved belemnite and *Gryphaea* calcite from the Sundance Sea provides temperature estimates independent of the isotopic composition of seawater. Compared with prior studies, our approach offers several key advantages: clumped isotope thermometry enables higher-accuracy temperature reconstruction than single-isotope methods; reconstruction of $\delta^{18}O_{SW}$ within a semi-enclosed seaway removes the need to assume a global seawater $\delta^{18}O$ of −1‰; and $^{87}Sr/^{86}Sr$ analysis provides a robust means to evaluate the relative influence of open-ocean versus terrestrial-sourced waters.

The principal contribution of this study is a refined interpretation of the Oxfordian shaped by extreme warmth, with the Sundance Sea reaching or exceeding temperatures comparable to modern tropical extremes. Such elevated temperatures likely had profound impacts on the regional Oxfordian ecosystem, increasing the risk of

Figure 6. Temporal variation in temperature throughout the Jurassic. All clumped isotope and $\delta^{18}O$ temperatures are calculated from belemnites using both N. T. Anderson et al. (2021) and Kele et al. (2015), assuming an open ocean average of −1‰ for the Jurassic (Shackleton & Kennett, 1975). Abbreviations: OWI, Oxfordian Warm Interval. Other climate events are defined by Dera et al. (2011) and Bodin et al. (2015). T-OAE, Toarcian Oceanic Anoxic Event. MJCH, Middle Jurassic Cold House. MTCH, Middle Toarcian Cold House. LPCH, Late Pliensbachian Cold House. PTM, Pliensbachian Thermal Maximum. Age from the International Commission on Stratigraphy (2024). Data sets for oxygen and clumped isotopes are available in Supporting Information S1 (ST8).

25724525, 2026, 7, Downloaded from https://agupubs.onlinelibrary.wiley.com/doi/10.1029/2025PA005364 by Open Research - University Of East Anglia , Wiley Online Library on [13/08/2026]. See the Terms and Conditions (https://onlinelibrary.wiley.com/terms-and-conditions) on Wiley Online Library for rules of use; OA articles are governed by the applicable Creative Commons License

degradation through reduced oxygen availability and heat stress, with consequent effects on ecosystem composition, function, and biodiversity. Moreover, the near-landlocked Sundance Sea may have exerted a moderating influence on the climate of adjacent terrestrial regions, providing new insight into regional climate dynamics during the Late Jurassic.

This study also constrains key characteristics of the Sundance Sea, including its temperature and seawater isotopic composition. However, the present results also demonstrate that, even assuming no diagenetic bond reordering, interpretation of the clumped isotope record remains complex and robust reconstructions require consideration of multiple interacting controls. Despite these challenges, this investigation demonstrates the effectiveness of the Δ_{47} proxy for quantitatively reconstructing Jurassic climate and provides a framework for future studies aimed at reconstructing and understanding interactions between regional seas and broader climatic systems.

Inclusion in Global Research Statement

We would like to thank W. E. Worrell, University of Wyoming, for their support and local insight during the field expedition, A. F. J. Wroblewski (University of Wyoming) for guidance on paleogeographic reconstructions, and the Bureau of Land Management for the collection of "common" invertebrate fossils on their land for use in the study.

Conflict of Interest

The authors declare no conflicts of interest relevant to this study.

Availability Statement

All data and supporting information is available at Reynolds et al. (2026).

Acknowledgments
This work was supported by the Natural Environment Research Council and the ARIES Doctoral Training Partnership (Grant NE/S007334/1). A. Oldroyd, University of Cardiff, is thanked for thin section preparation; as well as J. Diepenbrock, University of Wyoming, for their assistance in providing additional samples from the Warm Springs site. We would like to thank the three anonymous reviewers for their insightful comments and constructive suggestions, which improved the quality of this manuscript.

References

Allen, P. A., & Allen, J. R. (2013). *Basin analysis: Principles and application to petroleum play assessment*. John Wiley & Sons Ltd.

Alosiri, Y., Imberger, J., & Falconer, R. A. (2011). Mixing and flushing in the Persian Gulf (Arabian Gulf). *Journal of Geophysical Research*, *116*, eC3029. https://doi.org/10.1029/2010JC006769

Anderson, F. A., & Arthur, M. A. (1983). Stable isotopes of oxygen and carbon and their application to sedimentologic and paleoenvironmental problems. In M. A. Arthur, T. F. Anderson, I. R. Kaplan, J. Veizer, & L. S. Land (Eds.), *Stable isotopes in sedimentary geology*. SEPM.

Anderson, N. T., Kelson, J. R., Kele, S., Daëron, M., Bonifacie, M., Horita, J., et al. (2021). A unified clumped isotope thermometer calibration (0.5–1,100°C) using carbonate-based standardization. *Geophysical Research Letters*, *48*(7), e2020GL092069. https://doi.org/10.1029/2020GL092069

Arkell, W. J. (1956). *Jurassic geology of the world.* Oliver & Boyd.

Barbin, V. (1995). Cathodoluminescence of carbonates: New applications in geology and archaeology. *Scanning Microscopy*, *9*, 9. https://digitalcommons.usu.edu/microscopy/vol1995/iss9/9

Bernasconi, S. M., Daëron, M., Bergmann, K. D., Bonifacie, M., Meckler, A. N., Affek, H. P., et al. (2021). InterCarb: A community effort to improve interlaboratory standardization of the carbonate clumped isotope thermometer using carbonate standards. *Geochemistry, Geophysics, Geosystems*, *22*, e2020GC009588. https://doi.org/10.1029/2020GC009592

Bodin, S., Meissner, P., Janssen, N. M. M., Steuber, T., & Mutterlose, J. (2015). Large igneous provinces and organic carbon burial: Controls on global temperature and continental weathering during the Early Cretaceous. *Global and Planetary Change*, *133*, 238–253. https://doi.org/10.1016/j.gloplacha.2015.09.001

Brenner, R. L., & Davies, D. K. (1974). Oxfordian sedimentation in western interior United States. *American Association of Petroleum Geologists Bulletin*, *58*(3), 407–428. https://doi.org/10.1306/83D91407-16C7-11D7-8645000102C1865D

Cochran, J. K., Landman, N. H., Turekian, K. K., Michard, A., & Schrag, D. P. (2003). Paleoceanography of the late cretaceous (Maastrichtian) western interior seaway of North America: Evidence from Sr and O isotopes. *Palaeogeography, Palaeoclimatology, Palaeoecology*, *191*(1), 45–64. https://doi.org/10.1016/S0031-0182(02)00642-9

Curley, A. N., Petersen, S. V., Fricke, H., & Gleason, J. (2025). Insight into climate and hydrology of the late cretaceous western interior basin from clumped isotope Paleothermometry and strontium isotopes. *Earth and Planetary Science Letters*, *651*, e119180. https://doi.org/10.1016/j.epsl.2024.119180

Danise, S., & Holland, S. M. (2018). A sequence stratigraphic framework for the middle to late Jurassic of the Sundance Seaway, Wyoming: Implications for correlation, basin evolution, and climate change. *Journal of Geology*, *126*(4), 371–405. https://doi.org/10.1086/697692

Danise, S., Price, G. D., Alberti, M., & Holland, S. M. (2020). Isotopic evidence for partial geochemical decoupling between a Jurassic epicontinental sea and the open ocean. *Gondwana Research*, *82*, 97–107. https://doi.org/10.1016/j.gr.2019.12.011

Dennis, P. F., Myhill, D. J., Marca, A., & Kirk, R. (2018). Clumped isotope evidence for episodic, rapid flow of fluids in a mineralized fault system in the Peak District, UK. *Journal of the Geological Society*, *176*(3), 447–461. https://doi.org/10.1144/jgs2016-117

Dera, G., Brigaud, B., Monna, F., Laffont, R., Pucéat, E., Deconinck, J. F., et al. (2011). Climatic ups and downs in a disturbed Jurassic world. *Geology*, *39*(3), 215–218. https://doi.org/10.1130/G31579.1

El Meknassi, S., Dera, G., De Rafelis, M., Brahmi, C., Lartaud, F., Hodel, F., et al. (2020). Seawater $^{87}Sr/^{86}Sr$ ratios along continental margins: Patterns and processes in open and restricted shelf domains. *Chemical Geology*, *558*, e119874. https://doi.org/10.1016/j.chemgeo.2020.119874

Fan, M., & Carrapa, B. (2014). Late cretaceous-early Eocene Laramide uplift, exhumation, and basin subsidence in Wyoming: Crustal responses to flat slab subduction. *Tectonics*, *33*(4), 509–529. https://doi.org/10.1002/2012TC003221

Foster, G. L., Royer, D., & Lunt, D. (2017). Future climate forcing potentially without precedent in the last 420 million years. *Nature Communications*, *8*(1), e14845. https://doi.org/10.1038/ncomms14845

Gerritzen, C. T., Goderis, S., James, H. F., & Snoeck, C. (2024). Optimizing Zr-doped MC-ICP-MS sample-standard bracketing to simultaneously determine $^{87}Sr/^{86}Sr$ and $\delta^{88}Sr$ for high sample throughput. *Spectrochimica Acta Part B: Atomic Spectoscopy*, *217*, e106955. https://doi.org/10.1016/j.sab.2024.106955

Ghosh, P., Adkins, J., Affek, H., Balta, B., Guo, W., Schauble, E. A., et al. (2008). ^{13}C–^{18}O bonds in carbonate minerals: A new kind of paleothermometer. *Geochimica et Cosmochimica*, *70*(6), 1439–1456. https://doi.org/10.1016/j.gca.2005.11.014

Gottardi, R., Adams, L. M., Borrok, D., & Teixeira, B. (2019). Hydrocarbon source rock characterization, burial history, and thermal maturity of the Steele, Niobrara and Mowry formations at Teapot Dome, Wyoming. *Marine and Petroleum Geology*, *100*, 326–340. https://doi.org/10.1016/j.marpetgeo.2018.11.012

Gröcke, D. R., Price, G. D., Ruffell, A. H., Mutterlose, J., & Baraboshkin, E. (2003). Isotopic evidence for late Jurassic-early cretaceous climate change. *Palaeogeography, Palaeoclimatology, Palaeoecology*, *202*(1–2), 97–118. https://doi.org/10.1016/S0031-0182(03)00631-X

Guo, W., Mosenfelder, J. L., Goddard, W. A., & Eiler, J. M. (2009). Isotopic fractionations associated with phosphoric acid digestion of carbonate minerals: Insights from first-principles theoretical modeling and clumped isotope measurements. *Geochimica et Cosmochimica Acta*, *73*(24), 7203–7225. https://doi.org/10.1016/j.gca.2009.05.071

Harris, R., McCall, R., Randall, O., Tawang, M. H. B., Williams, R., Fairman, J. G., & Schultz, D. M. (2017). Climate change during the Triassic and Jurassic. *Geology Today*, *33*(6), 210–215. https://doi.org/10.1111/gto.12210

Hemingway, J. D., & Henkes, G. A. (2021). A disordered kinetic model for clumped isotope bond reordering in carbonates. *Earth and Planetary Science Letters*, *566*, e116962. https://doi.org/10.1016/j.epsl.2021.116962

Henkes, G. A., Passey, B. H., Grossman, E. L., Shenton, B. J., Yancey, T. E., & Pérez-Huerta, A. (2018). Temperature evolution and the oxygen isotope composition of Phanerozoic oceans from carbonate clumped isotope thermometry. *Earth and Planetary Science Letters*, *490*, 40–50. https://doi.org/10.1016/j.epsl.2018.02.001

Hoffmann, R., & Stevens, K. (2019). The palaeobiology of belemnites–Foundation for the interpretation of rostrum geochemistry. *Biological Reviews*, *95*(1), 94–123. https://doi.org/10.1111/brv.12557

Husinec, A., & Read, J. F. (2007). The late Jurassic Tithonian, a greenhouse phase in the middle Jurassic–Early Cretaceous cool mode: Evidence from the cyclic Adriatic platform, Croatia. *Sedimentology*, *54*(2), 317–337. https://doi.org/10.1111/j.1365-3091.2006.00837.x

Imlay, R. W. (1947). Marine Jurassic of Black Hills area, South Dakota, and Wyoming. *AAPG Bulletin*, *31*(2), 227–273. https://doi.org/10.1306/3D933947-16B1-11D7-8645000102C1865D

Imlay, R. W. (1980). *Jurassic Paleobiogeography of the conterminous United States in its continental setting* (Vol. 1062, pp. 1–134). Geological Survey Professional Paper. Retrieved from https://pubs.usgs.gov/pp/1062/report.pdf

Imlay, R. W. (1982). *Jurassic (Oxfordian and late Callovian) ammonites from the western interior region of the United States* (Vol. 1232, pp. 1–44). Geological Survey Professional Paper. Retrieved from https://pubs.usgs.gov/pp/1232/report.pdf

International Commission on Stratigraphy. (2024). Stratigraphy v2024/12. Retrieved from https://stratigraphy.org/ICSchart/ChronostratChart2024-12.pdf

Jenkyns, H. C., Schouten-Huibers, L., Schouten, S., & Damsté, J. S. S. (2012). Warm middle Jurassic-early cretaceous temperatures from the southern ocean. *Climate of the Past*, *8*(1), 215–226. https://doi.org/10.5194/cp-8-215-2012

Jin, T., Huntington, K. W., Wen, Y., Gu, X., Schauer, A. J., & Zhang, L. (2024). Clumped isotope records of terrestrial temperatures during the Middle Jurassic (180-150 Ma) in East China. *Palaeogeography, Palaeoclimateology, Palaecology*, *637*, e112014. https://doi.org/10.1016/j.palaeo.2024.112014

Jones, C. E. (2001). Seawater strontium isotopes, oceanic anoxic events, and seafloor hydrothermal activity in the Jurassic and Cretaceous. *American Journal of Science*, *301*(2), 112–149. https://doi.org/10.2475/ajs.301.2.112

Jones, M. M., Petersen, S. V., & Curley, A. N. (2022). A tropically hot mid-cretaceous North American western interior seaway. *Geology*, *50*(8), 954–958. https://doi.org/10.1130/G49998.1

Keeling, R. G., Körtzinger, A., & Gruber, N. (2010). Ocean deoxygenation in a warming world. *Annual Review of Marine Science*, *2*(1), 463–493. https://doi.org/10.1146/annurev.marine.010908.163855

Kele, S., Breitenbach, S. F. M., Capezzuoli, E., Meckler, A. N., Ziegler, M., Millan, I. M., et al. (2015). Temperature dependence of oxygen- and clumped isotope fractionation in carbonates: A study of travertines and Tufas in the 6–95°C temperature range. *Geochimica et Cosmochimica Acta*, *168*, 172–192. https://doi.org/10.1016/j.gca.2015.06.032

Kowallis, B. J., Christiansen, E. H., Deino, A., Peterson, F., Turner, C., Kunk, M. J., & Obradovich, J. D. (1998). The age of the Morrison Formation. *Modern Geology*, *22*, 235–260.

Kramchaninov, A., Chernyshev, I. V., & Shatagin, K. N. (2012). Isotope analysis of strontium by multicollector inductively-coupled plasma mass spectrometry: High-precision combined measurement of $^{88}Sr/^{86}Sr$ and $^{87}Sr/^{86}Sr$ isotope ratios. *Journal of Analytical Chemistry*, *67*(14), 1084–1092. https://doi.org/10.1134/S1061934812140067

Kvale, E. P., Johnson, G. D., Mickelson, D. L., Keller, K., Furer, L. C., & Archer, A. W. (2001). Middle Jurassic (Bajocian and Bathonian) dinosaur megatracksites, Bighorn Basin, Wyoming, U.S.A. *PALAIOS*, *16*(3), 233–254. https://doi.org/10.1669/0883-1351(2001)016<0233:MJBABD>2.0.CO;2

Kvale, E. P., Mickelson, D. L., Hasiotis, S. T., & Johnson, G. D. (2004). The history of dinosaur footprint discoveries in Wyoming with emphasis on the bighorn Basin. *Ichnos*, *11*(1–2), 3–9. https://doi.org/10.1080/10420940490428823

Le Grande, A. N., & Schmidt, G. A. (2006). Global gridded data set of the oxygen isotopic composition in seawater. *Geophysical Research Letters*, *33*, eL12604. https://doi.org/10.1029/2006GL026011

Locarnini, R. A., Mishonov, A. V., Baranova, O. K., Boyer, T. P., Zweng, M. M., Garcia, H., et al. (2019). *World Ocean Atlas 2018, volume 1: Temperature*. NOAA Atlas NESDIS.

Looser, N., Petschnig, P., Hemmingway, J. D., Fernandez, A., Grafulha, L. M., Perez-Huerta, A., et al. (2023). Thermally-induced clumped isotope resetting in belemnite and optical calcites: Towards material-specific kinetics. *Geochimica et Cosmochimica Acta*, *350*, 1–15. https://doi.org/10.1016/j.gca.2023.03.030

Macarewich, S. I., Poulsen, C. J., & Montañez, I. P. (2021). Simulation of oxygen isotopes and circulation in a late carboniferous epicontinental sea with implications for proxy records. *Earth and Planetary Science Letters*, *559*, e116770. https://doi.org/10.1016/j.epsl.2021.116770

Massare, J. A., Wahl, W. R., Ross, M., & Connely, M. V. (2013). Palaeoecology of the marine reptiles of the redwater shale member of the Sundance formation (Jurassic) of central Wyoming, USA. *Geological Magazine*, *151*(1), 167–182. https://doi.org/10.1017/S0016756813000472

25724525, 2026, 7, Downloaded from https://agupubs.onlinelibrary.wiley.com/doi/10.1029/2025PA005364 by Open Research - University Of East Anglia , Wiley Online Library on [13/08/2026]. See the Terms and Conditions (https://onlinelibrary.wiley.com/terms-and-conditions) on Wiley Online Library for rules of use; OA articles are governed by the applicable Creative Commons License

McArthur, J. M., Howarth, R. J., Shields, G. A., & Zhou, Y. (2020). Strontium isotope stratigraphy. In F. M. Gradstein, J. G. Ogg, M. D. Schmitz, & G. M. Ogg (Eds.), *Geologic time scale 2020*. Elsevier.

McMullen, S. K., Holland, S. M., & O'Keefe, F. R. (2014). The occurrence of vertebrate and invertebrate fossils in a sequence stratigraphic context: The Jurassic Sundance formation, Bighorn Basin, Wyoming, USA. *PALAIOS*, *29*(6), 277–294. https://doi.org/10.2110/pal.2013.132

Müller, I. A., Fernandez, A., Radke, J., van Dijk, J., Bowen, D., Schwieters, J., & Bernasconi, S. M. (2017). Carbonate clumped isotope analyses with the long-integration dual-inlet (LIDI) workflow: Scratching at the lower sample weight boundaries. *Rapid Communications in Mass Spectrometry*, *31*(12), 1057–1066. https://doi.org/10.1002/rcm.7878

Neely, J. (1937). Stratigraphy of the Sundance Formation and related Jurassic rocks in Wyoming and their petroleum aspects. *AAPG Bulletin*, *21*(6), 715–770. https://doi.org/10.1306/3D932ED4-16B1-11D7-8645000102C1865D

Nesterov, O., Temimi, M., Fonseca, R., Nelli, N. R., Addad, Y., Bosc, E., & Abida, R. (2021). Validation and statistical analysis of the group for high resolution sea surface temperature data in the Arabian Gulf. *Oceanologia*, *63*(4), 497–515. https://doi.org/10.1016/j.oceano.2021.07.001

Paleolatitude. (2025). Paleolatitude. Retrieved from https://paleolatitude.org

Parcell, W. C., & Williams, M. K. (2005). Mixed sediment deposition in a retro-arc foreland basin: Lower Ellis Group (M. Jurassic), Wyoming and Montana, U.S.A. *Sedimentary Geology*, *177*(3–4), 175–194. https://doi.org/10.1016/j.sedgeo.2005.02.007

Passey, B. H., & Henkes, G. (2012). Carbonate clumped isotope bond reordering and geospeedometry. *Earth and Planetary Science Letters*, *351–352*, 223–236. https://doi.org/10.1016/j.epsl.2012.07.021

Paxton, R. B., Andrews, J. E., Dennis, P. F., Marca, A. D., & Holmden, C. (2023). Concretionary cementation of a Scottish Middle Jurassic sandstone by hot, Paleocene fluids: A clumped isotope study. *Journal of the Geological Society*, *180*(3), jgs2022-175. https://doi.org/10.1144/jgs2022-175

Pearce, C. R., Parkinson, I. J., Gaillardet, J., Charlier, B. L. A., Mokadem, F., & Burton, K. W. (2015). Reassessing the stable ($\delta^{88}/^{86}$Sr) and radiogenic (^{87}Sr/^{86}Sr) strontium isotopic composition of marine inputs. *Geochimica et Cosmochimica Acta*, *157*, 125–146. https://doi.org/10.1016/j.gca.2015.02.029

Peterson, F. (1994). Sand dunes, sabkhas, streams, and shallow seas: Jurassic paleogeography in the southern part of the western interior basin. In M. V. Caputo, J. A. Peterson, & K. J. Franczyk (Eds.), *Mesozoic systems of the Rocky Mountain region*.

Pipiringos, G. N. (1957). Startigraphy of the sundance, nugget, and Jem formations in the Laramie Basin, Wyoming. *The Geological Survey of Wyoming*.

Pipiringos, G. N. (1968). Correlation and nomenclature of some Triassic and Jurassic rocks in south-central Wyoming. *U.S. Geological Survey Professional Paper*, *594-D*, 1–26. https://pubs.usgs.gov/pp/0594d/report.pdf

Pipiringos, G. N., & O'Sullivan, R. B. (1978). Principal unconformities in Triassic and Jurassic rocks, western interior United States–A preliminary survey. *Geological Survey Professional Paper*, *1035-A*, 1–29. https://pubs.usgs.gov/pp/1035a/report.pdf

Poulton, T. P. (1984). The Jurassic of the Canadian western interior, from 49°N latitude to the Beaufort Sea. *Canadian Society of Petroleum Geologists*, *9*, 15–41. https://ags.aer.ca/publications/atlas-western-canada-sedimentary-basin

Price, G. D., Bajnai, D., & Fiebig, J. (2020). Carbonate clumped isotope evidence for latitudinal seawater temperature gradients and the oxygen isotope composition of early cretaceous seas. *Palaeogeography, Palaeoclimatology, Palaeoecology*, *552*, e109777. https://doi.org/10.1016/j.palaeo.2020.109777

Price, G. D., Baker, S. J., Van der Velde, J., & Clemence, M. E. (2016). High-resolution carbon cycle and seawater temperature evolution during the early Jurassic (Sinemurian-Early Pliensbachian). *Geochemistry, Geophysics, Geosystems*, *17*(10), 3917–3928. https://doi.org/10.1002/2016GC006541

Price, G. D., Főzy, I., & Pálfy, J. (2016). Carbon cycle history through the Jurassic–Cretaceous boundary: A new global δ^{13}C stack. *Palaeogeography, Palaeoclimatology, Palaeoecology*, *451*, 46–61. https://doi.org/10.1016/j.palaeo.2016.03.016

Price, G. D., Heszler, B., Charlton, L.-M. T., & Cox, J. (2023). A climate perturbation at the middle–late Jurassic transition? Evaluating the isotopic evidence from south-central England. *Palaeogeography, Palaeoclimatology, Palaeoecology*, *628*, e111755. https://doi.org/10.1016/j.palaeo.2023.111755

Reeside, J. B. (1919). Some American Jurassic Ammonites of the genera *Quenstedticeras, Cardioceras*, and *Amoeboceras*, family *Cardioceratidae*. *US Geological Survey*, 5–38.

Reynolds, R., Jerrett, R., Marca, A., Bernasconi, S., Davies, M., Nowell, G., et al. (2026). A tropically hot late Jurassic North American Sundance Sea: Evidence for the Oxfordian warm interval [Dataset]. *University of Plymouth Research Repository*. https://doi.org/10.24382/1d114a19-9d2f-4cc7-80dd-3a61db8910d6

Sælen, G., Doyle, P., & Talbot, M. R. (1996). Stable-isotope analyses of belemnite rostra from the Whitby Mudstone Fm., England: Surface water conditions during deposition of a marine black shale. *PALAIOS*, *11*(2), 97–117. https://doi.org/10.2307/3515065

Scheiner, F., Holcova, K., Milovsky, R., & Kuhnert, H. (2018). Emperature and isotopic composition of seawater in the epicontinental sea (Central Paratethys) during the middle Miocene climate transition based on Mg/Ca, δ^{18}O and δ^{13}C from foraminiferal tests. *Palaeogeography, Palaeoclimatology, Palaeoecology*, *495*, 60–71. https://doi.org/10.1016/j.palaeo.2017.12.027

Schueth, J. D., Wroblewski, A., & Minor, K. P. (2025). Revised paleogeographic maps of the North American western interior seaway: Applying integrated approaches for predictive reconstructions and recognizing bias from lack of data. *AAPG Bulletin*, *109*(7), 991–1025. https://doi.org/10.1306/06302524031

Schwarz, E., Ramirez, M., Lazo, D. G., Veiga, G. D., Isla, M. I., Echevarria, C., et al. (2022). A review on depositional systems, bioevents and paleogeography of the Valanginian-Hauterivian Neuquén Sea: Refining sedimentary and biological signals linked to the dynamics of Epeiric seas. *Earth-Science Reviews*, *234*, e104224. https://doi.org/10.1016/j.earscirev.2022.104224

Sellwood, B. W., & Jenkyns, H. C. (1975). Basins and swells and the evolution of an Epeiric sea: (Pliensbachian–Bajocian of Great Britain). *Journal of the Geological Society*, *131*(4), 373–388. https://doi.org/10.1144/gsjgs.131.4.0373

Seton, M., Müller, R. D., Zahirovic, S., Gaina, C., Torsvik, T., Shephard, G., et al. (2012). Global continental and ocean basin reconstructions since 200 Ma. *Earth-Science Reviews*, *113*(3–4), 212–270. https://doi.org/10.1016/j.earscirev.2012.03.002

Shackleton, N., & Kennett, J. (1975). *Paleotemperature history of the Cenozoic and the initiation of Antarctic glaciation: Oxygen and carbon isotope analyses in DSDP sites 277, 279 and 281* (Vol. 29, pp. 743–755). Initial Reports of the Deep Sea Drilling Project. Retrieved from https://api.semanticscholar.org/CorpusID:58902065

Song, H., Wignall, P. B., Chu, D., Tong, J., Sun, Y., Song, H., et al. (2014). Anoxia/high temperature double whammy during the Permian-Triassic marine crisis and its aftermath. *Nature Scientific Reports*, *4*(1), e4132. https://doi.org/10.1038/srep04132

Stampfli, G. M., & Borel, G. D. (2002). A plate tectonic model for the Paleozoic and Mesozoic constrained by dynamic plate boundaries and restored synthetic oceanic isochrons. *Earth and Planetary Science Letters*, *196*(1–2), 17–33. https://doi.org/10.1016/s0012-821x(01)00588-x

Stevens, A. L., Balgord, E. A., & Carrapa, B. (2016). Revised exhumation history of the Wind River Range, WY, and implications for Laramide tectonics. *Tectonics*, *35*(5), 1121–1136. https://doi.org/10.1002/2016tc004126

25724525, 2026, 7, Downloaded from https://agupubs.onlinelibrary.wiley.com/doi/10.1029/2025PA005364 by Open Research - University Of East Anglia , Wiley Online Library on [13/08/2026]. See the Terms and Conditions (https://onlinelibrary.wiley.com/terms-and-conditions) on Wiley Online Library for rules of use; OA articles are governed by the applicable Creative Commons License

Suzuki, M., & Nagasawa, H. (2013). Mollusk shell structures and their formation mechanism. *Canadian Journal of Zoology*, *91*(6), 349–366. https://doi.org/10.1139/cjz-2012-0333

Tang, C. M., & Bottjer, D. J. (1996). Long-term faunal stasis without evolutionary coordination: Jurassic benthic marine paleocommunities, western interior, United States. *Geology*, *24*(9), 815–818. https://doi.org/10.1130/0091-7613(1996)024<0815:ltfswe>2.3.co;2

Uhlir, D. M., Akers, A., & Vondra, C. F. (1988). Tidal inlet sequence, Sundance formation (upper Jurassic), north-central Wyoming. *Sedimentology*, *35*(5), 739–752. https://doi.org/10.1111/j.1365-3091.1988.tb01248.x

Ullmann, C. V., & Korte, C. (2015). Diagenetic alteration in low-Mg calcite from macrofossils: A review. *Geological Quarterly*, *59*, 3–20. https://doi.org/10.7306/gq.1217

Ullmann, C. V., Thibault, N., Ruhl, M., Hesselbo, S. P., & Korte, C. (2014). Effect of a Jurassic oceanic anoxic event on belemnite ecology and evolution. *Proceedings of the National Academy of Sciences of the United States of America*, *111*(28), 10073–10076. https://doi.org/10.1073/pnas.1320156111

USGS. (2025). National geological map database. Retrieved from https://ngmdb.usgs.gov/Geolex/Units/WindyHill_11198.html

Valdes, P. J., Scotese, C. R., & Lunt, D. J. (2021). Deep ocean temperatures through time. *Climate of the Past*, *17*(4), 1483–1506. https://doi.org/10.5194/cp-17-1483-2021

Veizer, J. (1989). Strontium isotopes in seawater through time. *Annual Review of Earth and Planetary Sciences*, *17*(1), 141–167. https://doi.org/10.1146/annurev.ea.17.050189.001041

Vickers, M. L., Bajnai, D., Price, G. D., Linckens, J., & Fiebig, J. (2019). Southern high-latitude warmth during the Jurassic-Cretaceous: New evidence from clumped isotope thermometry. *Geology*, *47*(8), 724–728. https://doi.org/10.1130/G46263.1

Vickers, M. L., Bernasconi, S. M., Ullmann, C. V., Lode, S., Looser, N., Morales, L. G., et al. (2021). Marine temperatures underestimated for past greenhouse climate. *Scientific Reports*, *11*(1), e19109. https://doi.org/10.1038/s41598-021-98528-1

Vickers, M. L., Fernandez, A., Hesselbo, S. P., Price, G. D., Bernasconi, S. M., Lode, S., et al. (2020). Unravelling middle to late Jurassic palaeoceanographic and palaeoclimatic signals in the Hebrides Basin using belemnite clumped isotope thermometry. *Earth and Planetary Science Letters*, *546*, e116401. https://doi.org/10.1016/j.epsl.2020.116401

Wang, T., He, S., Chen, Y., Aitchison, J. C., Zhang, Q., Li, G., et al. (2025). Were late Jurassic climate fluctuations responses to Pangea breakup? Evidence from isotopic analysis of belemnite rostra from the eastern Tethyan Ocean. *GSA Bulletin*, *137*(3–4), 986–1005. https://doi.org/10.1130/B37313.1

Wang, T., Hoffmann, R., He, S., Zhang, Q., Li, G., Randrianaly, H. N., et al. (2023). Early Cretaceous climate for the southern Tethyan Ocean: Insights from the geochemical and paleoecological analyses of extinct cephalopods. *Global and Planetary Change*, *229*, e104220. https://doi.org/10.1016/j.gloplacha.2023.104220

Wang, T., Yang, P., He, S., Hoffmann, R., Xhang, Q., Farnsworth, A., et al. (2024). Absolute age and temperature of belemnite rostra: Constraints on the Early Cretaceous cooling event. *Global and Planetary Change*, *233*, e104353. https://doi.org/10.1016/j.gloplacha.2023.104353

Wierzbowski, H., Anczkiewicz, R., Pawlak, J., Rogov, M. A., & Zuznetsov, A. B. (2017). Revised middle–upper Jurassic strontium isotope stratigraphy. *Chemical Geology*, *466*, 239–255. https://doi.org/10.1016/j.chemgeo.2017.06.015

Wierzbowski, H., Bajnai, D., Wacker, U., Rogov, M. A., Fiebig, J., & Tesakova, E. M. (2018). Clumped isotope record of salinity variations in the Subboreal Province at the Middle–Late Jurassic transition. *Global and Planetary Change*, *167*, 172–189. https://doi.org/10.1016/j.gloplacha.2018.05.014

Woodward, S. C., Thomas, D. J., Grossman, E. L., Olszewski, T. D., Yancy, T. E., Miller, B. V., & Raymond, A. (2013). Radiogenic isotope composition of carboniferous seawater from North American epicontinental seas. *Palaeogeography, Palaeoclimatology, Palaeoecology*, *370*, 51–63. https://doi.org/10.1016/j.palaeo.2012.11.018

Wroblewski, A. F.-J., & Morris, E. A. (2022). Unconformity generation and the shift from storm-dominated to tide-dominated processes in a Jurassic Retroarc foreland basin: Insights from ichnology. *Depositional Record*, *9*(2), 253–299. https://doi.org/10.1002/dep2.215

Xianghui, L., Wang, J., Rasbury, T., Zhou, M., Wei, Z., & Zhang, C. (2020). Early Jurassic climate at atmospheric CO2 concentration in the Sichuan paleobasin, southwestern China. *Climate of the Past*, *16*, 2055–2074. https://doi.org/10.5194/cp-16-2055-2020

Zhou, T., Qi, L., Fan, H., & Yin, R. (2020). An optimized protocol for high precision measurement of 87Sr/86Sr using a Neptune plus multi-collector inductively coupled plasma mass spectrometer: Evaluation of different cone combinations for Sr isotope determination. *Analytical Methods*, *12*(32), 4089–4096. https://doi.org/10.1039/D0AY00845A

Zuchuat, V., Steel, E., Mulligan, R. P., Collins, D. S., & Mattias-Green, J. A. (2022). Tidal dynamics in palaeo-seas in response to changes in physiography, tidal forcing and bed shear stress. *Sedimentology*, *69*(4), 1861–1890. https://doi.org/10.1111/sed.12975

References From the Supporting Information

Alberti, M., Fürsich, F. T., & Pandey, D. K. (2012). The Oxfordian stable isotope record ($\delta^{18}O$, $\delta^{13}C$) of belemnites, brachiopods, and oysters from the Kachchh Basin (western India) and its potential for palaeoecologic, palaeoclimatic, and palaeogeographic reconstructions. *Palaeogeography, Palaeoclimatology, Palaeoecology*, *344–345*, 49–68. https://doi.org/10.1016/j.palaeo.2012.05.018

Armendariz, M., Rosales, I., Badenas, B., Pinuela, L., Aurell, M., & Garcıa-Ramos, J. C. (2013). An approach to estimate Lower Jurassic seawater oxygen-isotope composition using $\delta^{18}O$ and Mg/Ca ratios of belemnite calcites (early Pliensbachian, northern Spain). *Terra Nova*, *25*(6), 439–445. https://doi.org/10.1111/ter.12054

Bailey, T. R., Rosenthal, Y., McArthur, J. M., van de Schootbrugge, B., & Thirlwall, M. F. (2003). Paleoceanographic changes of the Late Pliensbachian–Early Toarcian interval: A possible link to the genesis of an Oceanic Anoxic Event. *Earth and Planetary Science Letters*, *212*(3–4), 307–320. https://doi.org/10.1016/S0012-821X(03)00278-4

Benito, M. I., & Reolid, M. (2012). Belemnite taphonomy (Upper Jurassic, Western Tethys) part II: Fossil–diagenetic analysis including combined petrographic and geochemical techniques. *Palaeogeography, Palaeoclimatology, Palaeoecology*, *358–360*, 89–108. https://doi.org/10.1016/j.palaeo.2012.06.035

Brigaud, B., Pucéat, E., Pellenard, P., Vincent, B., & Joachimski, M. M. (2008). Climatic fluctuations and seasonality during the late Jurassic (Oxfordian–Early Kimmeridgian) inferred from $\delta^{18}O$ of Paris Basin oyster shells. *Earth and Planetary Science Letters*, *273*(1–2), 58–67. https://doi.org/10.1016/j.epsl.2008.06.015

Coimbra, R., & Olóriz, F. (2012). Contrast comparison of differential diagenetic pathways of Lower Tithonian carbonate materials from the Betic Cordillera (S. Spain): Evidence for physico-chemical paleo-seawater properties. *Palaeogeography, Palaeoclimatology, Palaeoecology*, *321–322*, 65–79. https://doi.org/10.1016/j.palaeo.2012.01.018

Dera, G., & Donnadieu, Y. (2011). Modeling evidence for global warming, Arctic seawater freshening, and sluggish oceanic circulation during the Early Toarcian anoxic event. *Paleoceanography*, *27*, ePA2211. https://doi.org/10.1029/2012PA002283

25724525, 2026, 7, Downloaded from https://agupubs.onlinelibrary.wiley.com/doi/10.1029/2025PA005364 by Open Research - University Of East Anglia , Wiley Online Library on [13/08/2026]. See the Terms and Conditions (https://onlinelibrary.wiley.com/terms-and-conditions) on Wiley Online Library for rules of use; OA articles are governed by the applicable Creative Commons License

Dera, G., Pucéat, E., Pellenard, P., Neige, P., Delsate, D., Joachimski, M. M., et al. (2009). Water mass exchange and variations in seawater temperature in the NW Tethys during the early Jurassic: Evidence from neodymium and oxygen isotopes of fish teeth and belemnites. *Earth and Planetary Science Letters*, *286*(1–2), 198–207. https://doi.org/10.1016/j.epsl.2009.06.027

Fernandez, A., Korte, C., Ullmann, C. V., Looser, N., Wohlwend, S., & Bernasconi, S. M. (2021). Reconstructing the magnitude of Early Toarcian (Jurassic) warming using the reordered clumped isotope compositions of belemnites. *Geochimica et Cosmochimica*, *293*, 308–327. https://doi.org/10.1016/j.gca.2020.10.005

Főzy, I., Janssen, N. M. M., & Price, G. D. (2011). High-resolution ammonite, belemnite and stable isotope record from the most complete Upper Jurassic section of the Bakony Mts (Transdanubian Range, Hungary). *Geologica Carpathica*, *62*(5), 413–433. https://doi.org/10.2478/v10096-011-0030-y

Fürsich, F. T., Singh, I. B., Joachimski, M., Krumm, S., Schlirf, M., & Schlirf, S. (2005). Palaeoclimate reconstructions of the Middle Jurassic of Kachchh (western India): An integrated approach based on palaeoecological, oxygen isotopic, and clay mineralogical data. *Palaeogeography, Palaeoclimatology, Palaeoecology*, *217*(3–4), 289–309. https://doi.org/10.1016/j.palaeo.2004.11.026

Gómez, J. J., Canales, M. L., Ureta, S., & Goy, A. (2009). Palaeoclimatic and biotic changes during the Aalenian (Middle Jurassic) at the southern Laurasian Seaway (Basque–Cantabrian Basin, northern Spain). *Palaeogeography, Palaeoclimatology, Palaeoecology*, *275*(1–4), 14–27. https://doi.org/10.1016/j.palaeo.2009.01.009

Gómez, J. J., Goy, A., & Canales, M. L. (2008). Seawater temperature and carbon isotope variations in belemnites linked to mass extinction during the Toarcian (early Jurassic) in Central and Northern Spain. Comparison with other European sections. *Palaeogeography, Palaeoclimatology, Palaeoecology*, *258*(1–2), 28–58. https://doi.org/10.1016/j.palaeo.2007.11.005

Hesselbo, S. P., Gröcke, D. R., Jenkyns, H. C., Bjerrum, C. J., Farrimond, P., Morgans Bell, H. S., & Green, O. R. (2000). Massive dissociation of gas hydrate during a Jurassic oceanic anoxic event. *Nature*, *406*(6794), 392–395. https://doi.org/10.1038/35019044

Jenkyns, H. C., & Macfarlane, S. (2021). The chemostratigraphy and environmental significance of the Marlstone and Junction Bed (Beacon Limestone, Toarcian, Lower Jurassic, Dorset, UK). *Geological Magazine*, *159*(3), 357–371. https://doi.org/10.1017/S0016756821000972

Jenkyns, H. C., Jones, C. E., Gröcke, D. R., Hesselbo, S. P., & Parkinson, D. N. (2002). Chemostratigraphy of the Jurassic System: Applications, limitations and implications for palaeoceanography. *Journal of the Geological Society*, *159*(4), 351–378. https://doi.org/10.1144/0016-764901-130

Jones, C. E. (1992). *Strontium isotopes in Jurassic and Early Cretaceous seawater*. University of Oxford. Retrieved from https://ora.ox.ac.uk/objects/uuid:fe3733bd-8e31-4bba-a78b-6d8275a0075f/download_file?file_format=pdf&hyrax_fileset_id=m9e9bd92c617057f44d47bdb44c953158&safe_filename=602830203.pdf&type_of_work=Thesis

Korte, C., & Hesselbo, S. P. (2011). Shallow marine carbon and oxygen isotope and elemental records indicate icehouse-greenhouse cycles during the early Jurassic. *Paleoceanography*, *26*(4), PA4219. https://doi.org/10.1029/2011PA002160

Korte, C., Hesselbo, S. P., Ullmann, C. V., Dietl, G., Ruhl, M., Schweigert, G., & Thibault, N. (2015). Jurassic climate mode governed by ocean gateway. *Nature Communications*, *6*(1), e10015. https://doi.org/10.1038/ncomms10015

Letulle, T., Suan, G., Daëron, M., Rogov, M., Lécuyer, C., Vinçon-Laugier, A., et al. (2022). Clumped isotope evidence for early Jurassic extreme polar warmth and high climate sensitivity. *Climate of the Past*, *18*(3), 435–448. https://doi.org/10.5194/cp-18-435-2022

Li, Q., McArthur, J. M., & Atkinson, T. C. (2012). Lower Jurassic belemnites as indicators of palaeo-temperature. *Palaeogeography, Palaeoclimatology, Palaeoecology*, *315–316*, 38–45. https://doi.org/10.1016/j.palaeo.2011.11.006

Longinelli, A., & Selmo, E. (2003). Isotopic composition of precipitation in Italy: A first overall map. *Journal of Hydrology*, *270*(1–2), 75–88. https://doi.org/10.1016/S0022-1694(02)00281-0

Mangenot, X., Gasparrini, M., Rouchon, V., & Boniface, M. (2018). Basin-scale thermal and fluid flow histories revealed by carbonate clumped isotopes (Δ_{47})–Middle Jurassic carbonates of the Paris Basin depocenter. *Sedimentology*, *65*(1), 123–150. https://doi.org/10.1111/sed.12427

McArthur, J. M., Donovan, D. T., Thirlwall, M. F., Fouke, B. W., & Mattey, D. (2000). Strontium isotope profile of the early Toarcian (Jurassic) oceanic anoxic event, the duration of ammonite biozones, and belemnite palaeotemperatures. *Earth and Planetary Science Letters*, *179*(2), 269–285. https://doi.org/10.1016/S0012-821X(00)00111-4

McArthur, J. M., Howarth, R. J., & Shields, G. A. (2001). Strontium isotope stratigraphy: LOWESS Version 3: Best fit to the marine Sr-isotope curve for 0–509 Ma and accompanying look-up table for deriving numerical age. *Journal of Geology*, *109*, 155–170. https://doi.org/10.1086/319243

Metodiev, L., & Koleva-Rekalova, E. (2008). Stable isotope records ($\delta^{18}O$ and $\delta^{13}C$) of Lower-Middle Jurassic belemnites from the Western Balkan Mountains (Bulgaria): Palaeoenvironmental application. *Applied Geochemistry*, *23*(10), 2845–2856. https://doi.org/10.1016/j.apgeochem.2008.04.010

Nunn, E. V., & Price, G. D. (2010). Late Jurassic (Kimmeridgian–Tithonian) stable isotopes ($\delta^{18}O$, $\delta^{13}C$) and Mg/Ca ratios: New palaeoclimate data from Helmsdale, northeast Scotland. *Palaeogeography, Palaeoclimatology, Palaeoecology*, *292*(1–2), 325–335. https://doi.org/10.1016/j.palaeo.2010.04.015

Padden, M., Weissert, H., & de Rafelis, M. (2001). Evidence for late Jurassic release of methane from gas hydrate. *Geology*, *29*(3), 223–226. https://doi.org/10.1130/0091-7613(2001)029<0223:efljro>2.0.co;2

Peterson, J. A. (1954). Marine Upper Jurassic, Eastern Wyoming. *AAPG Bulletin*, *38*(4), 463–507. https://doi.org/10.1306/5CEADEF3-16BB-11D7-8645000102C1865D

Peucker-Ehrenbrink, B., Miller, M. W., Arsouze, T., & Jeandel, C. (2010). Continental bedrock and riverine fluxes of strontium and neodymium isotopes to the oceans. *Geochemistry, Geophysics, Geosystems*, *11*(3), 1–22. https://doi.org/10.1029/2009GC002869

Podlaha, O., Mutterlose, J., & Veizer, J. (1998). Preservation of $\delta^{18}O$ and $\delta^{13}C$ in belemnite rostra from the Jurassic/Early Cretaceous successions. *American Journal of Science*, *298*(4), 324–347. https://doi.org/10.2475/ajs.298.4.324

Price, G. D. (2010). Carbon-isotope stratigraphy and temperature change during the Early–Middle Jurassic (Toarcian–Aalenian), Raasay, Scotland, UK. *Palaeogeography, Palaeoclimatology, Palaeoecology*, *285*(3–4), 255–263. https://doi.org/10.1016/j.palaeo.2009.11.018

Price, G. D., & Page, K. N. (2008). A carbon and oxygen isotopic analysis of molluscan faunas from the Callovian-Oxfordian boundary at Redcliff Point, Weymouth, Dorset: Implications for belemnite behaviour. *Proceedings of the Geologists' Association*, *119*(2), 153–160. https://doi.org/10.1016/S0016-7878(08)80315-X

Price, G. D., & Rogov, M. A. (2009). An isotopic appraisal of the Late Jurassic greenhouse phase in the Russian Platform. *Palaeogeography, Palaeoclimatology, Palaeoecology*, *273*(1–2), 41–49. https://doi.org/10.1016/j.palaeo.2008.11.011

Price, G. D., & Teece, C. (2010). Reconstruction of Jurassic (Bathonian) palaeosalinity using stable isotopes and faunal associations. *Journal of the Geological Society*, *167*(6), 1199–1208. https://doi.org/10.1144/0016-76492010-029

Riboulleau, A., Baudin, F., Daux, V., Hantzpergue, P., Renard, M., & Zakharov, V. (1998). Évolution de la paléotempérature des eaux de la plate-forme russe au cours du Jurassique supérieur. *Comptes Rendus de l'Academie des Sciences - Series IIA: Earth and Planetary Science*, *326*(4), 239–246. https://doi.org/10.1016/S1251-8050(97)86813-9

25724525, 2026, 7, Downloaded from https://agupubs.onlinelibrary.wiley.com/doi/10.1029/2025PA005364 by Open Research - University Of East Anglia , Wiley Online Library on [13/08/2026]. See the Terms and Conditions (https://onlinelibrary.wiley.com/terms-and-conditions) on Wiley Online Library for rules of use; OA articles are governed by the applicable Creative Commons License

Rosales, I., Quesada, S., & Robles, S. (2004). Paleotemperature variations of early Jurassic seawater recorded in geochemical trends of belemnites from the Basque–Cantabrian basin, northern Spain. *Palaeogeography, Palaeoclimatology, Palaeoecology*, *203*(3–4), 253–275. https://doi.org/10.1016/S0031-0182(03)00686-2

Teichert, B. M. A., & Luppold, F. W. (2013). Glendonites from an early Jurassic methane seep — Climate or methane indicators? *Palaeogeography, Palaeoclimatology, Palaeoecology*, *390*, 81–93. https://doi.org/10.1016/j.palaeo.2013.03.001

van de Schootbrugge, B., Bailey, T. R., Rosenthal, Y., Katz, M. E., Wright, J. D., Miller, K. G., et al. (2005). Early Jurassic climate change and the radiation of organic-walled phytoplankton in the Tethys Ocean. *Paleobiology*, *31*(1), 73–97. https://doi.org/10.1666/0094-8373(2005)031<0073:EJCCAT>2.0.CO;2

Veizer, J., Ala, D., Azmy, K., Bruckschen, P., Buhl, D., Bruhn, F., et al. (1999). $^{87}Sr/^{86}Sr$, $\delta^{13}C$ and $\delta^{18}O$ evolution of Phanerozoic seawater. *Chemical Geology*, *161*(1–3), 59–88. https://doi.org/10.1016/S0009-2541(99)00081-9

Wierzbowski, H. (2002). Detailed oxygen and carbon isotope stratigraphy of the Oxfordian in Central Poland. *International Journal of Earth Sciences*, *91*(2), 304–314. https://doi.org/10.1007/s005310100217

Wierzbowski, H., & Joachimski, M. (2007). Reconstruction of late Bajocian–Bathonian marine palaeoenvironments using carbon and oxygen isotope ratios of calcareous fossils from the Polish Jura Chain (central Poland). *Palaeogeography, Palaeoclimatology, Palaeoecology*, *254*(3–4), 523–540. https://doi.org/10.1016/j.palaeo.2007.07.010

Wierzbowski, H., & Rogov, M. (2011). Reconstructing the palaeoenvironment of the Middle Russian Sea during the Middle–Late Jurassic transition using stable isotope ratios of cephalopod shells and variations in faunal assemblages. *Palaeogeography, Palaeoclimatology, Palaeoecology*, *299*(1–2), 250–264. https://doi.org/10.1016/j.palaeo.2010.11.006

Wierzbowski, H., Rogov, M., Matyja, B. A., Kiselev, D., & Ippolitov, A. (2013). Middle–Upper Jurassic (Upper Callovian–Lower Kimmeridgian) stable isotope and elemental records of the Russian Platform: Indices of oceanographic and climatic changes. *Global and Planetary Change*, *107*, 196–212. https://doi.org/10.1016/j.gloplacha.2013.05.011

Wilson, P. A., & Norris, R. D. (2001). Warm tropical ocean surface and global anoxia during the mid-cretaceous period. *Nature*, *412*(6845), 425–429. https://doi.org/10.1038/35086553

25724525, 2026, 7, Downloaded from https://agupubs.onlinelibrary.wiley.com/doi/10.1029/2025PA005364 by Open Research - University Of East Anglia , Wiley Online Library on [13/08/2026]. See the Terms and Conditions (https://onlinelibrary.wiley.com/terms-and-conditions) on Wiley Online Library for rules of use; OA articles are governed by the applicable Creative Commons License